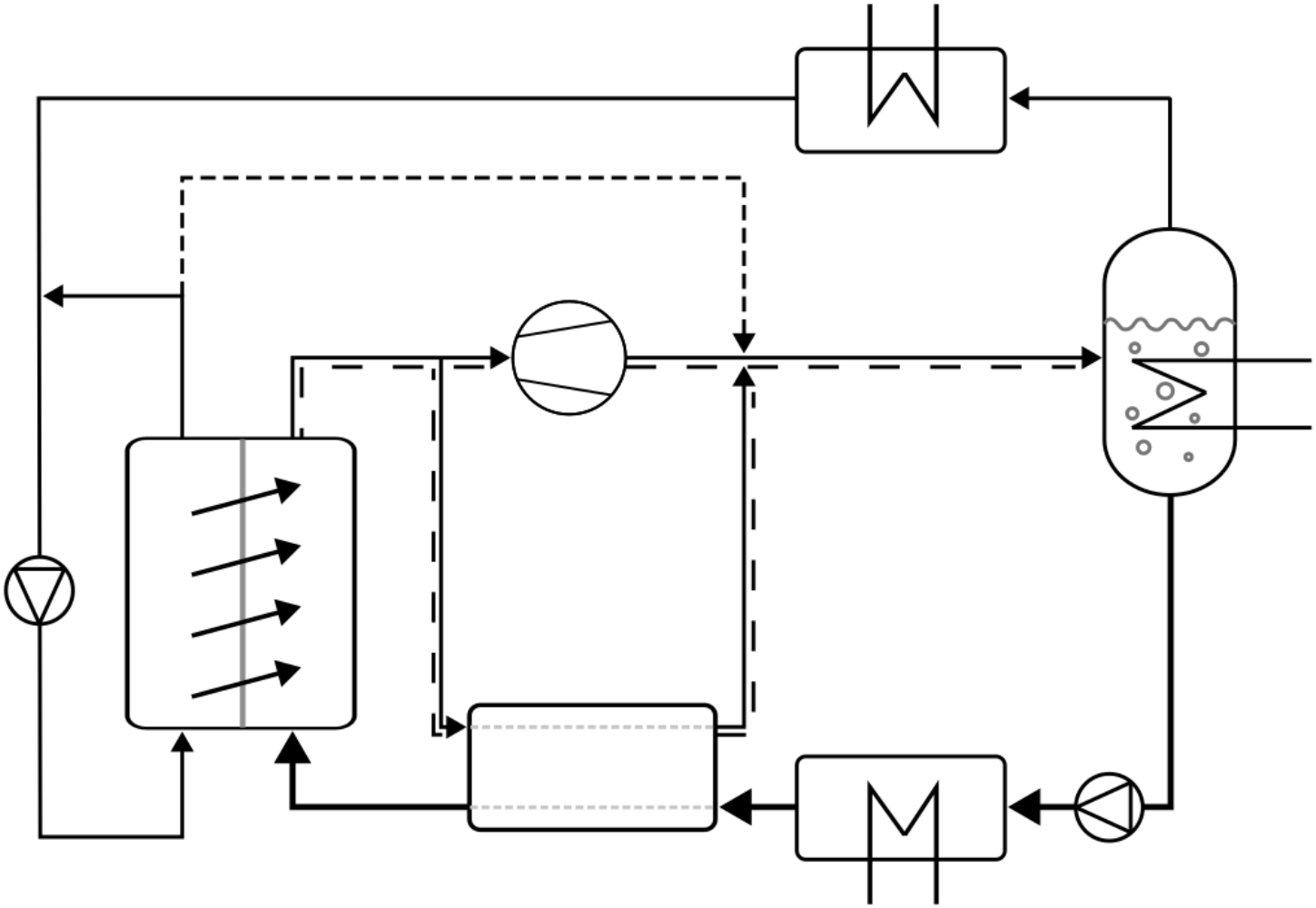

Analysis of Osmotic Heat Engine for Low Temperature Waste Heat Recovery

Low Temperature Waste Heat Recovery

Mikkel Ullits Thomsen

Thermal Energy and Process Engineering, TEPE4-1005, 2024-05

Master Thesis

AAU Energy
Aalborg University
http://www.aau.dk

AALBORG UNIVERSITY
STUDENT REPORT

Title:
Analysis of Osmotic Heat Engine for Low Temperature Waste Heat Recovery

Theme:
Low Temperature Waste Heat Recovery

Project Period:
Spring Semester 2024

Project Group:
TEPE4-1005

Participant(s):
Mikkel Ullits Thomsen

Supervisor(s):
Kim Sørensen
Thomas Condra

Page Numbers: 57

Date of Completion:
May 31, 2024

Abstract:

This project examines the use of an Osmotic Heat Engine (OHE) to utilise low temperature waste heat (40°C − 60°C). The proposed system used NaCl as the solute and pure water as the solvent, as most current research revolves around organic salts and not much research has been conducted on systems using NaCl.
A membrane model was constructed to examine how the membrane is affected by variations of parameters, both in terms of fluid properties and properties related to the membrane itself. The membrane model is implemented in a closed loop system model to model the OHE process and once again examine the effect of individual parameters.
This led to an optimisation to examine the optimal performance of the system, which found that the optimal system efficiency was approximately 0.13% and found that the system generates approximately 3.5 times the amount of electricity supplied. However, in order to do this, the components have to be unreasonably large, which leads to the conclusion that the current solution is unfeasible for the purpose. This might change with further design modifications and research in the field.

Resumé

Dette projekt undersøger muligheden for at bruge "Pressure Retarded Osmosis" (PRO) til energigenvinding fra ultra lav temperatur spildvarme, altså i temperaturintervallet $40°C - 60°C$. Udtrykket PRO dækker over osmose, hvor siden med høj saltkoncentration tryksættes. På denne måde kan trykforøgelsen på væsken, som gennemtrænger membranen, udnyttes til at drive en turbine og dermed generere strøm. Denne tilgang bruges flere steder i verden til energiproduktion, hvor der er adgang til både salt- og ferskvand, for eksempel ved flodudmundinger. For at drive processen skal der altså være mulighed for at skabe en forskel i osmotisk tryk henover membranen, da dette er drivkraften for systemet.

For at udnytte varme til at drive processen kan systemet lukkes, således at opblandingen af solvent og koncentrat, efter at have passeret turbinen igen adskilles til en koncentreret opløsning og rent solvent. Den rene solvent pumpes til lavtrykssiden af membranen, hvor den igen gennemtrænger membranen til højtrykssiden. Denne proces gentages, og en kreds der udnytter processen kaldes en "Osmotic Heat Engine" (OHE). I forbindelse med forsking i lukkede OHE kredse har fokus været på organiske salte som solut. Derfor undersøger dette projekt muligheden for at bruge natriumklorid (NaCl), samt hvordan dette påvirker kredsen og effektiviteten af dette. Det danner grundlag for følgende problemformulering:

> *Hvor effektiv er en OHE, der bruger NaCl som solut, til at udnytte lavtemperatur restvarme til strømproduktion, og er en NaCl-baseret OHE en holdbar løsning til varmegenvinding ved lave temperaturer?*

For at undersøge dette blev der opbygget en model af en hulfiber-membran. Den valgte membran til formålet er produceret af Toyobo, hvor data på membranen er sammenlagt af en artikel, der undersøger membranens vand- og saltpermeabilitet, såvel som de strukturelle parametre, og et datablad fra Toyobo, som beskriver membranens dimensioner. Det er blevet undersøgt hvordan saltgennemtrængningen igennem membranen og dennes effekttæthed påvirkes af tryk, saltkoncentration og masseflow på henholdsvis lavtrykssiden og højtrykssiden af membranen. Derudover er det blevet undersøgt hvordan permeabilitet og strukturelle egenskaber påvirker ydeevnen.

På baggrund af den udarbejdede membranmodel er der blevet opstillet en model af et OHE system. Resultaterne fra membranmodellen gav grundlag for at indsætte en forbindelse fra siden med rent vand (lavtrykssiden) til siden med saltvand (højtrykssiden). Forbindelsen er nødvendig, da saltet som strømmer over membranen ellers ville ophobes og forøge saltkoncentrationen på lavtrykssiden. Saltophobningen kan dermed undgås ved kontinuerligt at pumpe en andel af vandet fra lavtrykssiden til højtrykssiden. For at undersøge ydeevnen af systemet blev der igen udført en analyse, hvor der blev opstillet to parametre til at bedømme ydeevnen af systemet:

- Systemets totale virkningsgrad er den første parameter. Denne er baseret på hvor meget strøm, der produceres i forhold til det totale energiinput, både i form af varme og strøm.
- Systemets "Coefficient of Performance" (COP) er den anden parameter og er beregnet som et forhold imellem hvor meget strøm der produceres og hvor meget strøm der tilføres. Hvor virkningsgraden af systemet også tog hensyn til den tilførte varme, anses varmen altså som "gratis" energi i forbindelse med COP.

Den parametriske analyse af hele systemet gav anledning til at lave en optimering for at undersøge den optimale ydeevne for systemet med den givne opsætning. Det blev i den forbindelse identificeret at de vigtigste faktorer var relateret til koncentrationen på højtrykssiden af membranen, og trykket på lavtrykssiden af membranen. Der var dog ikke grundlag for at optimere disse, eftersom analysen viste at koncentration på højtrykssiden skulle være så høj som mulig og trykket på lavtrykssiden så lavt som mulig, hvilket værdierne allerede var defineret som i modellen. Derudover blev trykket på højtrykssiden også fastsat så højt som muligt, da dette er gavnligt for systemet. Optimeringen blev i stedet foretaget på andelen af vand pumpet fra lavtryks- til højtrykssiden, koncentration på højtrykssiden af membranen og masseflow ind i membranen på henholdsvis lavtryks- og højtrykssiden.

På baggrund af optimeringen viste det sig, at den totale virkningsgrad for systemet er 0.13%, hvilket vurderes til at være meget lav, imens systemets COP er beregnet til ≈ 3.46. Systemet leverer altså stadig mere strøm end det forbruger. Temperaturen på det restvarmen er sat til 65°C, hvilket betyder at mætningstrykket er 0.25 bar. Derfor er densiteten af dampen i fordamperen 0.16 kg/m^3, hvilket betyder der skal produceres 9 m^3/s damp. Det medfører at komponenterne i systemet skal være relativt store, for at producere den beregnede effekt på 5.9 kW. Det vurderes derfor at teknologien, med NaCl som solut, skal forbedres markant for at fremstå som en god løsning til restvarmegenvinding. Løsningsforslagene kunne både omhandle andre former for solut såvel som eventuelle designændringer til systemet der kan forbedre driften og virkningsgraden.

Preface

This project is written as the final thesis on the fourth semester of the Thermal Energy and Process Engineering on Aalborg University.

Acknowledgements

I wish to express my gratitude to Danfoss and SaltPower, that have spent numerous resources on orchestrating several meetings and visits to company sites in Mariager where SaltPower installations were presented and explained. The experiences have been invaluable and an interesting look into the corporate world of research.

Søren Gundtoft in particular should be thanked for sparring sessions with me and facilitating communication with external sources, which has been of great help to further expand my understanding of the topics in question.

Similarly, I want to thank my supervisors Kim Sørensen and Thomas Condra who have provided excellent support as I have developed my knowledge on a previously unknown field of thermodynamic cycles. Furthermore, their guidance have helped me to improve the quality of the thesis and elevate my academic level.

Reading Instructions

For references in the project, the Harvard method is used. The references show the last name of the author and the year of the publication. In the case of two or more authors, et al. is written after the name of the first author. The names of all authours, the title of the paper and links to the sources are listed in the bibliography. Throughout the project, both figures, table and equations are assigned a number based on the order in which they appear. Figure 1.2 for example can be found in chapter 1 and is the second figure in the given chapter. In some graphs in the report, for example $x10^{-6}$ is written besides an axis. This means, that the values on the axis should be multiplied with the order of magnitude written over the axis to get the correct value.

Mikkel Ullits Thomsen
<mikkth21@student.aau.dk>

Abbreviations

Abbreviation	Definition
AL-DS	Active Layer - Draw Solution
AL-FS	Active Layer - Feed Solution
CP	Concentration Polarisation
CCC	Carbon Carrier Cycle
CFD	Computational Fluid Dynamics
COP	Coefficient of Performance
ECP	External Concentration Polarisation
FDM	Finite Difference Method
FO	Forward Osmosis
ICP	Internal Concentration Polarisation
OHE	Osmotic Heat Engine
PEX	Pressure Exchanger
PRO	Pressure Retarded Osmosis
RED	Reverse Electrodialysis
RO	Reverse Osmosis
SMA	Shape Memory Alloy

Nomenclature

Symbol	Definition	Unit
d	Diameter	m
f	Friction factor	–
h	Specific enthalpy	kJ/kg
i	Van 't Hoff Factor	–
k	Mass transfer coefficient	m/s
k_p	Pressure loss constant	–
$\dot{m}$	Mass flow	kg/s
r	Radius	m
s	Salinity	g/kg
t	Thickness	m
u	Velocity	m/s
x	Mass fraction	–
z	Distance	m
A	Area	m^2
A	Water permeability	$m^3/s/(m^2 \cdot bar)$
B	Salt permeability	$m^3/s/m^2$
C	Concentration	mol/L
D	Mass diffusivity	m^2/s
J	Flux	m/s
L	Length	m
MW	Molar weight	g/mol
PD	Power density	W/m^2
P	Power	W
P	Pressure	bar
Q	Heat flow	W
R	Gas constant	$L \cdot atm/(K \cdot mol)$
S	Structural parameter	µm
T	Temperature	K
W	Work	W
δ	Boundary layer thickness	m
ε_p	Porosity	–
ε_r	Surface roughness	m
ε_v	Void fraction	–
η	Efficiency	–
μ	Dynamic viscosity	$Pa \cdot s$
ν	Kinematic viscosity	m^2/s
π	Osmotic pressure	atm
ρ	Density	kg/m^3

Subscript and Superscript

Subscript and superscript	Definition
avg	Average
b	Bulk
D	Draw side
F	Feed side
fi	Inner fibre property
fo	Outer fibre property
eff	Effective
h	Hydraulic
HEX	Heat exchanger
HP	High pressure
i	Inner
L	Leakage
LP	Low pressure
m	Membrane
n	Nodal
PEX	Pressure exchanger
s	Salt
s	Shell side
sys	System
$turb$	Turbine
w	Water

Contents

Chapter 1

Introduction

In 2015, a legally binding treaty was introduced by the United Nations, which obligates all countries to reduce carbon emissions, such that the increase in global average temperature stays below 2K, relative to pre-industrial temperatures. According to United Nations (2023), this means that global greenhouse gas emissions must have peaked before 2025, and should have decreased by more than 40% in 2030.

At the time of writing this project, the green transition of the global society is very much in progress. A part of this transition revolves around phasing out fossil fuels, both in electricity producing facilities and in industrial processes. As nations strive to become low-carbon economies and reduce greenhouse gas emissions, new technologies are needed to replace fossil fuels. The most prevalent technologies to this day are wind and solar power, among others such as hydro and geothermal energy. While plenty of research is conducted to improve the efficiency of green technologies, many industrial processes generate vast amounts of waste heat. This excess heat is often either cooled into the atmosphere or to waterways. By doing so, potential energy savings are wasted.

Waste heat can be found in all temperature regimes, from temperatures relatively close to ambient temperatures and up to several hundred degrees above these. Luberti et al. (2022) examined the waste heat available in the EU between 40°C and 60°C and found the results listed in Table 1.1.

Temperature range [°C]	Waste heat [10^6 GJ]
< 40	548.3
$40 - 59$	6441.4
$60 - 79$	1042.2
$80 - 99$	290.0
$100 - 499$	132.2
$500 - 999$	97.8

Table 1.1: Description of waste heat available from power generation in the given temperature intervals. The data for the table is published by Luberti et al. (2022).

From table 1.1, it turned out that the available amount of waste heat from power generation by EU alone, summed up to more than $6400 \cdot 10^6$ GJ. For comparison, $6400 \cdot 10^6$ GJ is approximately ten times as much energy as the total electricity production of Denmark in 2022. (IEA 2023b)

The reason for the waste heat generation being so high from power generation, is due to the limitations of the Rankine cycle. Hence, a decrease in used fossil fuels will also result in a decrease of waste heat from this sector. However, according to IEA (2023a), the data centres constructed by Apple, Google, and Meta among others, are responsible for between 1-1.5% of global electricity consumption today. Oltmanns et al. (2020) states that about 90% of the electric energy supplied to a data centre can be recuperated through waste heat recovery. In 2021, the global electricity consumption was 25 543 TWh, which means that data centres, assuming 1% of electricity consumption, consumed 255 TWh, equal to the electricity consumption of Australia in the same year. (U.S. Energy Information Administration 2023) This is already a significant amount of energy, which is currently wasted, available for utilisation and as the digitalisation of nations continue, the electricity consumption of data centres, and therefore the generation of waste heat, is only expected to rise.

One approach to utilise the waste heat, is to convert it into electricity. For researchers and developers, this is a hot topic, and several technologies are already being examined and developed for this purpose. Kumar et al. (2019) examined the use of a Shape Memory Alloy (SMA) for electricity production. The technology works by using an alloy which contracts when heated and expands to its previous state when it cools back down. The contraction is used to create continuous rotation over a pulley and is then coupled to a generator and mounted on a hot pipe. As the alloy is heated it will contract, creating a rotating motion. When it cools down, the stretching allows it to move back to the hot zone, which resets the process. It was found that the technology was easily scalable, as several SMA units can be installed in succession, and a thermal efficiency of 1.5% could be reached for a waste heat temperature of 80°C, corresponding to a Carnot efficiency of about 10%. To achieve maximum efficiency of the system, the available heating and cooling should be at the exact temperatures to reach the full transition between the stretched and contracted states. Higher or lower temperatures reduce the Carnot efficiency of the system, limiting where the technology is applicable.

Micheli et al. (2021) studied a Carbon Carrier Cycle (CCC) which resembles an absorption machine, but with a turbine replacing the condenser and evaporator. The system uses Acetone and CO_2 and the study found that the CCC technology benefits from low absorber temperatures. Hence, this technology would be interesting if the heat sink temperature is lower than the atmospheric ambient temperature.

Reverse Electrodialyis (RED) is a technology which uses a salinity gradient to create an ion flux over a membrane which generates electricity. This was examined by Bevacqua et al. (2016) and Luo et al. (2012) using NH_4HCO_3 as the solute, as this changes into NH_3, CO_2 and water when heated. Palenzuela et al. (2018) did a performance analysis of RED with NaCl as the solute coupled with Multi-Effect Distillation and found that in this setup with an ideal membrane, an exergy efficiency of almost 31% could be reached.

Another approach to using a membrane is with an osmotic heat engine(OHE). As revealed by the name, the OHE works by the principle of osmosis. Osmosis describes molecule diffusion from a less concentrated solution over a semi permeable membrane to a more concentrated solution. Generally, osmosis can be separated in two technologies; forward osmosis and reverse osmosis. Reverse osmosis is the most widely used of the two and is used in several industries for filtration and desalination, among others. When doing reverse osmosis, a solution is pressurised, which results in fluid flow over the membrane. The solute will then freely flow through the membrane, while the solvent cannot pass.

Forward osmosis means that instead of promoting flow through pressurisation, the osmotic driving force is a concentration gradient, determined by the difference in concentration of solute

on each side of the membrane. This results in a difference of osmotic pressures over the membrane, which is defined as the pressure needed to stop the molecule permeating toward the side with a high concentration of solute. This principle is illustrated in Figure 1.1.

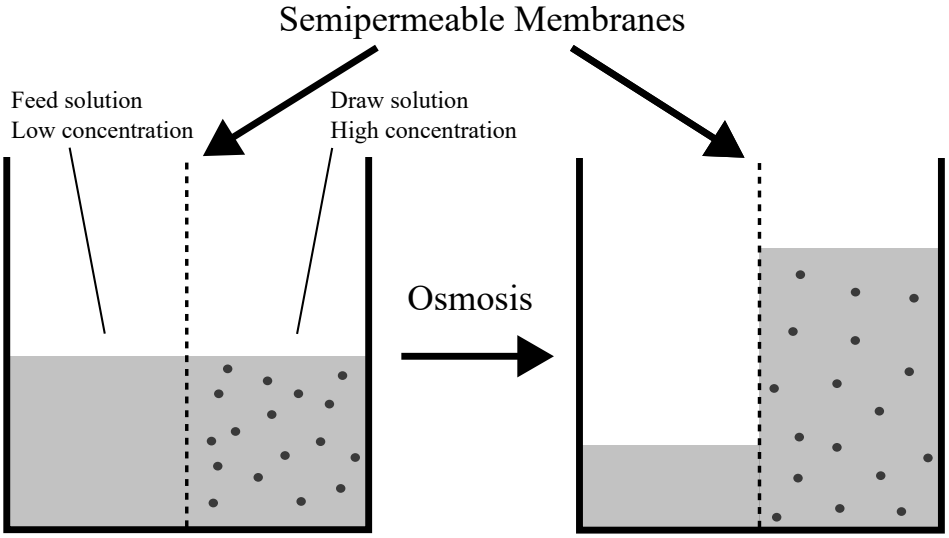

Figure 1.1: Illustration of the osmosis principle. On the left side of the figure, the system is shown before osmosis with a low concentration solution left of the membrane and a high concentration solution on the right of the membrane.

The water flows from the low solute concentration, also called the feed solution, to the high concentration, called the draw solution, resulting in an accumulation of fluid on the high concentration side; hence instead of concentrating the solute as with reverse osmosis, PRO dilutes the solute. If PRO is done in a closed container, it will lead to a pressure increase equal to the osmotic pressure on the draw side of the membrane. Using this pressure increase, electricity can then be generated using a turbine.

This project examines the use of an OHE to recover low temperature waste heat from industrial processes, as well as how this process is affected by internal parameters. Which internal parameters will be explained further throughout the report.

1.1 State of The Art

McCutcheon et al. (2006) examined desalination with NH_3-CO_2 forward osmosis and how the feed and the draw concentrations affect the performance of the process. It was carried out experimentally and used saline water with NaCl as the feed solution and ammonia salts with soluted CO_2 as the draw solution. It was found that the draw solution concentration affects the water flux of the osmosis process significantly. However, when the concentration of the draw solution is increased, less of the osmotic pressure driving force is utilised due to increased internal concentration polarisation, meaning that a concentration gradient inside and around the membrane reduces the potential for osmosis. This resulted in a decreased performance ratio, with the performance ratio defined as the experimental water flux divided with the theoretical water flux.

McGinnis et al. (2007) did a study of PRO using ammonia salts and soluted CO_2 as the draw solution with deionised water as the feed solution, since this eliminates the internal concentration polarisation effects and thus ultimately increases the performance of the membrane. In the study, it was found that the maximum power density for the membrane is reached when the hydraulic pressure is $\approx$ 50% of the osmotic pressure. However, it was also found that the engine efficiency increases as the difference between hydraulic pressure and osmotic pressure approaches zero. The maximum Carnot efficiency of the examined system proved to be around 16%, and the power output per membrane area reached more than $250 W/m^2$.

Al-Zainati et al. (2024) did a study on PRO using multiple stages of membranes, with freshwater as the feed solution and saline water as the draw solution. Systems were modelled with one, two and four membrane stages. The examined membranes are connected in series on the draw side, and are parallel connected on the feed side of the membrane. It was found that more stages generally yielded a higher efficiency. This was due to the decrease of internal concentrative concentration polarisation on each individual membrane, which led to an improved water flux.

Chintalacheruvu et al. (2023) examined how heat can be used to enhance PRO. The test was conducted with applied pressure from 0 to 8 bar, and the feed and draw solution temperatures was increased up to 50°C and compared to the performance at 20°C. From the tests, it was found that by heating both solutions, the power density almost doubled at 7.5 bar applied pressure. Furthermore, it was found that heating only the feed solution almost yielded the same results. Hence, the study concluded, that the supplied thermal energy is best used by heating the feed solution as more thermal energy is needed to also heat the draw solution. Furthermore, Einarsson and Wu (2021) did a review on the temperature dependency of PRO processes. They also found that heating the feed solution affected the flux more than heating the draw solution. However, it was also stated that while higher temperatures promoted the feed solution flux, it does increase the reverse salt flux, which could reduce the overall performance of the PRO process. While the increased reverse salt flux could be a factor reducing the efficiency of the PRO system.

Besides temperature and pressure, the salinity of both draw and feed solutions also affect the performance of the system. Madsen et al. (2017) investigated commercial membranes and their performance in hypersaline PRO at pressures of up to 70 bar. The draw concentration was varied from 0.6M (3.5 wt%) to 5M (24.7 wt%) and the feed concentration from 0 to to 2wt%. In this study, 'M' denotes molarity. Molarity is a measure of the concentration of the solute, describing the number of moles of solute per litre of solution. For the draw concentration variations, pure water was used as the feed solution. While varying the feed concentration, a 3M draw solution

was used. The study showed that the maximum power density increased linearly with an increase in the draw concentration, while an increase in feed salinity had a negative but nonlinear effect. Furthermore, the study compared Thin Film Composite (TFC) membranes and Cellulose Triacetate (CTA) membranes and found that the TFC membranes reached higher flux at lower pressures, while CTA mebranes showed higher pressure stability, resulting in higher power densities under higher pressure.
Rahman et al. (2023) did a review on the current level of development of PRO, comparing different types of membranes for use in PRO applications and the commercialisation potential of these. The comparison of studies found that for PRO, the membranes cover more than 40% of the total equipment costs. However, in the study it is also noted that this is expected to decrease as membrane technologies are improved, for example through the use of nanomaterials, as this is expected to improve the relation between power generation and membrane cost.
Liang et al. (2022) did a study on how the mass exchange limit can be determined for PRO systems. To do so, a pinch analysis was constructed to include every PRO module, creating a mass exchanger network. A minimum net osmotic pressure difference is introduced, which is used as a constraint for which streams can be interconnected. Through the study, it was discovered, that for the given setup, a minimum net osmotic pressure difference resulted in 74% recovery of ideal work output and that the optimal operating pressure is not necessarily 0.5 times the osmotic pressure difference, which is often assumed. Instead depends on the osmotic pressure of the inlet and outlet draw solution, the volumetric fraction of feed stream and the minimum net osmotic pressure difference.

According to the literature review, PRO technology demonstrates significant utilisation potential in various applications, including OHEs. While the technology is being thoroughly researched, a deeper understanding of OHEs and their working principles will require more knowledge about the PRO process, especially within closed systems. Although sodium chloride as a solute has been well-researched for open systems, the focus has been on organic salts for closed systems. The following problem analysis aims to delve deeper into this, hereby presenting the relevance of the project.

Chapter 2

Problem Analysis

2.1 Osmosis

Osmosis describes molecule diffusion from a less concentrated solution over a semi-permeable membrane to a more concentrated solution. The osmotic driving force is a concentration gradient, determined by the difference in solute concentrations on each side of the membrane. The concentration difference results in an equilibrium pressure difference over the membrane, commonly referred to as osmotic pressure. The osmotic pressure can be used in several ways, and in industry, three general principles of osmosis are used:

- **Forward osmosis (FO)**
  FO utilises the osmotic pressure difference to promote molecule flow over the membrane, which means that no pressure is applied to the fluid. Forward osmosis occurs everywhere in nature, and it is also occurring in the body, for example, in the intestines for the body to absorb nutrients, in the lungs where oxygen and CO_2 are exchanged, to clean the blood in the kidneys, among others. In the industry, forward osmosis is often used for desalination of seawater. This is done using seawater as the feed solution and a draw solution which has a higher osmotic pressure than seawater. The draw solution can then be distilled to collect fresh water.

- **Reverse osmosis (RO)**
  RO means that the diffusion of molecules occurs in the direction which is opposite to the osmotic pressure gradient. Therefore, hydraulic pressure must be applied to overcome the osmotic pressure difference. In industry, RO is widely used to "clean" mixtures, meaning that unwanted parts of the mixtures can be removed. This could be bacteria or particles ranging down to nanometres in size. RO is also used to remove chemical compounds, as well as desalination and making ultra pure water.

- **Pressure retarded osmosis (PRO)**
  PRO is a type of FO, where a hydraulic pressure gradient is applied opposite to the osmotic pressure gradient. However, the applied pressure still has to be lower than the osmotic pressure difference, such that the solvent molecules flow from the low-pressure zone to the high-pressure zone. By doing so, a potential for electricity production is created, since the osmotic pressure for some compounds is several hundred bar.

2.1.1 Osmotic Pressure

Understanding the concept of osmotic pressure is crucial to understand osmosis. As previously stated, the osmotic pressure represents the pressure required to cancel the molecular flow over a semipermeable membrane caused by a concentration gradient. Generally, the osmotic pressure can be described by the Van 't Hoff equation, shown by equation 2.1. (Chintalacheruvu et al. 2023)

$$\pi = i \cdot C \cdot R \cdot T \tag{2.1}$$

Where i, C, R and T describe the Van 't Hoff factor, solute concentration, the universal gas constant and temperature, respectively. The Van 't Hoff factor is a dimensionless parameter, which represents the number of ions formed per mole of the dissolved solute. For NaCl dissolved in water, the Van 't Hoff factor equals 2 as two ions form, depicted in Equation 2.2

$$\mathrm{NaCl} \rightarrow \mathrm{Na}^{+} + \mathrm{Cl}^{-} \tag{2.2}$$

It is however important to note that NaCl dissociates completely in water. In some cases, if the solvent does not fully dissociate into ions, the ideal Van 't Hoff factor might deviate from the real factor.

Figure 2.1 illustrates the calculated osmotic pressure in saline water, for concentrations ranging from 0.5M to 1.5M and temperatures ranging from 15°C to 60°C, using the Van 't Hoff equation.

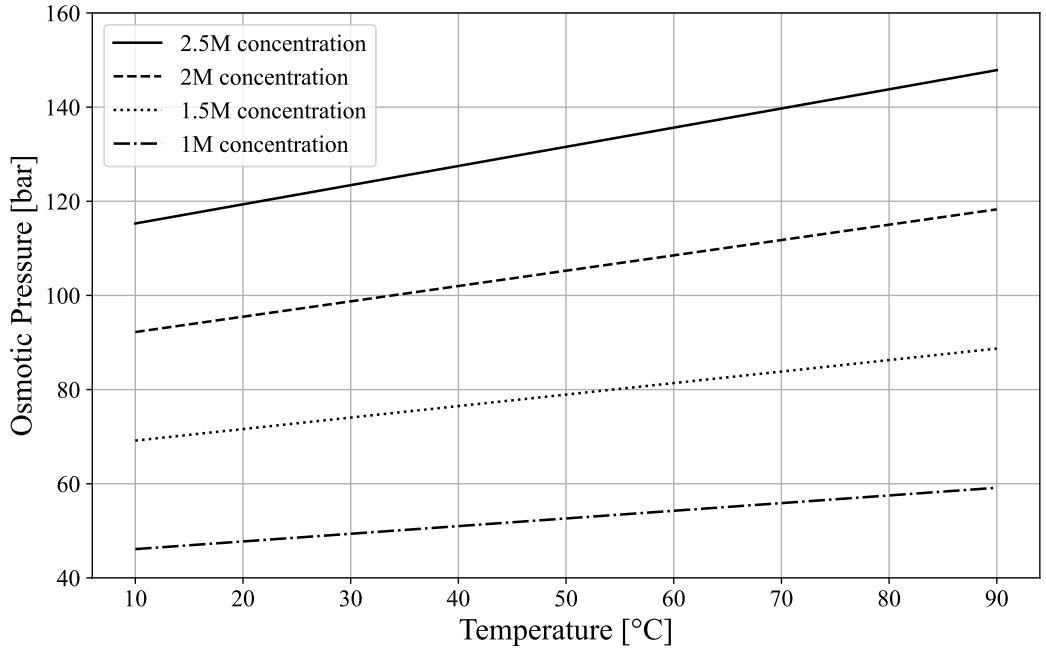

Figure 2.1: Osmotic pressure with NaCl as the solute and pure water as the solvent. The osmotic pressure is calculated using the Van 't Hoff equation.

On figure 2.1, the osmotic pressure is only illustrated up to a concentration of 2.5M, equivalent to about 139.8g NaCl per kg of water. The solubility of NaCl in water is higher than this, meaning that an even higher osmotic pressure can be reached. Figure 2.2 on page 8 illustrates the maximum solubility of NaCl in water, based on temperature. The figure is made based on data from Pavuluri (2014) which have been linearly regressed over the interval 10°C to 90°C.

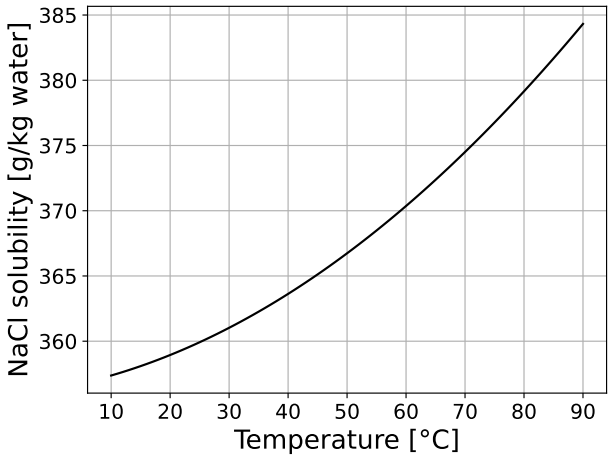

Figure 2.2: Solubility of NaCl in water based on temperature. The figure is based on data from Pavuluri (2014).

From the figure, it is shown that the solubility of NaCl in water varies from approximately 356 g/kg of water at 10°C to around 385 g/kg of water at 90°C. While pressure can affect solubility, it's considered negligible in this project, as previous research has shown that pressures below 50 MPa have less impact compared to temperature. (Sawamura et al. 2007)

As the Van 't Hoff equation uses concentration (mol/L) instead of salinity, the concentration is calculated by Equation 2.3:

$$C = \frac{s_s \cdot \rho_w}{MW_s} \tag{2.3}$$

Where s_s denotes the solubility of the salt, in this case NaCl, and MW_s denotes the molar weight of the salt, which for NaCl is 58.44 g/mol. An overview of the concentrations where precipitation occurs in a NaCl-water solution at temperatures ranging from 10°C − 90°C and the osmotic pressure for the saturated solution can be seen in Table 2.1.

Temperature [°C]	Saturated concentration [mol/L]	Osmotic pressure [bar]
10	6.872	316.9
20	6.908	329.8
30	6.955	343.4
40	7.014	357.7
50	7.086	372.9
60	7.170	389.0
70	7.266	406.1
80	7.374	424.1
90	7.496	443.3

Table 2.1: Description of the concentration of NaCl necessary to saturate a NaCl-water solution at temperatures varying between 10°C and 90°C. The osmotic pressure has been calculated for the solution, using the Van 't Hoff equation for osmotic pressure with the ideal Van 't Hoff factor $i = 2$.

As can be seen in Table 2.1, the impact of temperature on the maximum achievable osmotic pressure of a water-NaCl solution is readily apparent. This aligns with the principles outlined by

Van 't Hoff's equation, which takes into account both the solution temperature and concentration. As illustrated earlier in Figure 2.2, the maximum concentration increases with temperature. As an increase of temperature is directly represented in Equation 2.1 and indirectly through increased concentration, the significant increases of osmotic pressure in the table makes sense.

2.2 Membrane

A membrane is a layer of material which acts as a barrier. Membranes occur everywhere in nature, but membranes used in industrial processes are usually made synthetically. When working with osmosis, the membrane in focus is a so-called semipermeable membrane, meaning that some small particles or molecules can pass, while others cannot because they are too large. In other words, a semipermeable membrane permits selective mass transport through the size difference of different molecules.
Figure 2.3 illustrates the principle of a polymer based semipermeable membrane, where small particles pass while large particles are blocked.

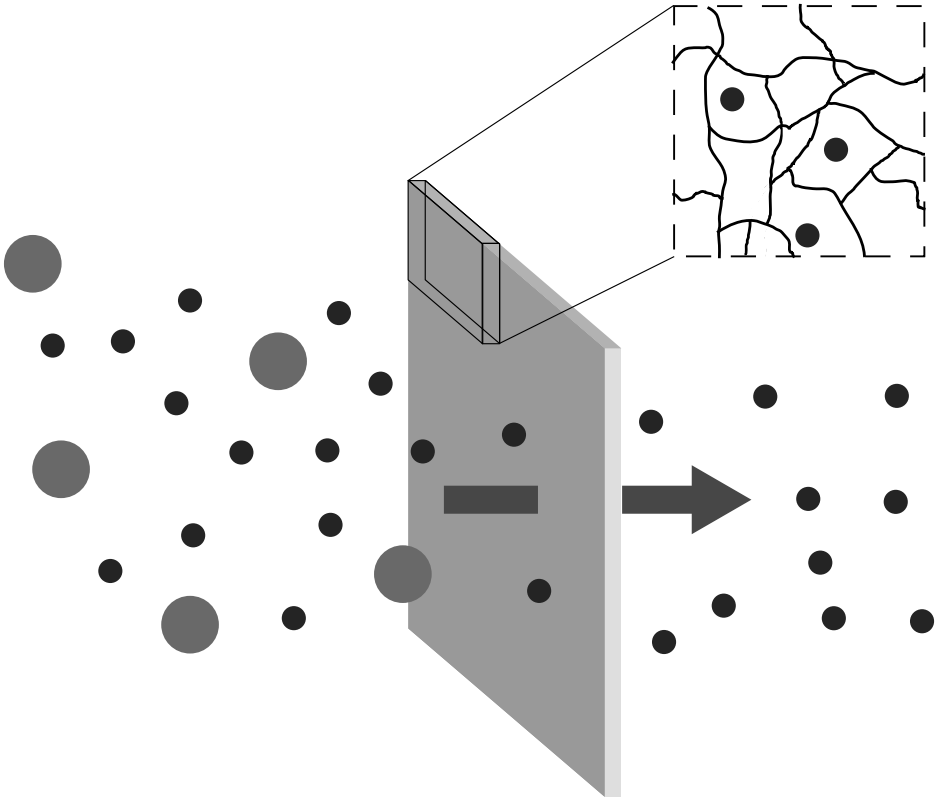

Figure 2.3: Illustration of semi-permeable membrane with the arrow representing the direction of flux. The figure shows how the small particles pass the membrane, while the large particles are held back. The upper right corner depicts a zoomed in view of the membrane to show the small particles passing through the gaps between strings of polymer.

In nature, membranes are made of organic materials, while commercial membranes usually are made of polymers. An illustration of the polymers and how the small particles fit through the gaps can be seen in the upper right corner of Figure 2.3. The flow over a membrane is typically denoted as the flux. Flux is defined as the flow over the membrane per square metre, which means that the higher the flux, the smaller the membrane is necessary to fulfil the requirements

of the system. The selectivity of the membrane is denoted as rejection and can be stated as a factor between 0 and 1. The rejection describes the membrane resistivity to reverse salt flux, in other words, how easily the salt passes through the membrane. The higher the rejection, the harder it is for the salt to pass.
Although the membrane structure varies based on the purpose of the membrane, any membrane subject to a large pressure difference between the feed and the draw side will need some kind of structural support. Because a membrane is made from a thin film called the selective layer, which is what permits selective mass transport, it cannot withstand high pressures on its own. As osmotic pressures can be very high for some solutions, structural support is necessary for the structural integrity of the membrane. Figure 2.4 illustrates how the membrane and support will be arranged, depending on the purpose of the membrane.

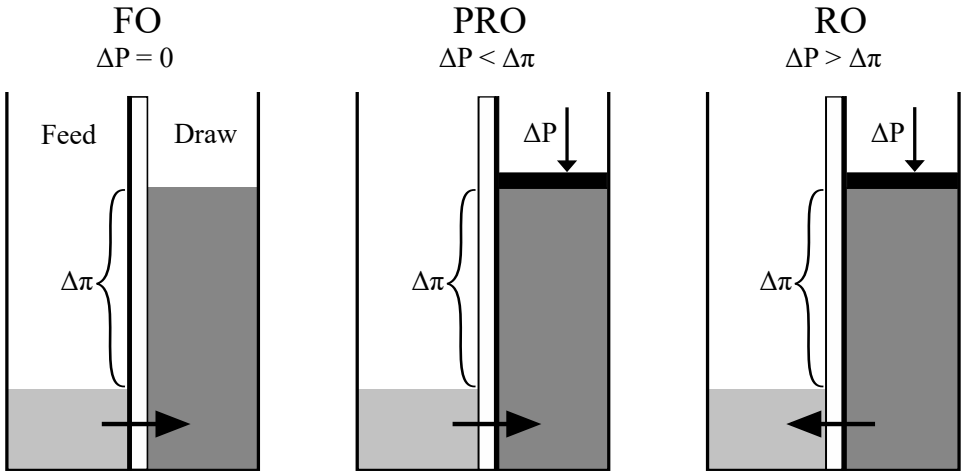

Figure 2.4: Illustration of the principles of FO, PRO and RO. On the illustration, the light grey represents the feed solution, and dark grey represents the concentrated draw solution. The horisontal arrow in the bottom depicts the direction of water flux and the bold line on the membrane represents the selective layer, while the white area on the membrane represents the porous support layer. $\Delta\pi$ is the osmotic pressure difference over them membrane, and ΔP is the applied hydraulic pressure.

As can be seen in Figure 2.4, the membrane will be aligned with the selective layer towards the feed solution for FO, whereas for both PRO and RO, the selective layer is placed in the opposite orientation. The reason for the opposite orientation is because of the large pressures, which the membrane has to withstand from the draw solution. From now on, the orientations will be referred to as AL-FS (active layer towards feed solution) when the active layer is oriented towards the feed solution, and AL-DS (active layer towards draw solution) when the active layer is oriented towards the draw solution.

2.2.1 Concentration Polarisation

Concentration Polarisation (CP) occurs due to selective transport over the membrane and describes a change of concentration that affects the osmotic pressure. Two types of concentration polarisation occur:

- **Internal concentration polarisation (ICP)** describes the concentration polarisation occuring internally in the porous support structure. As the fluid does not flow freely, a concentration gradient occurs, which is denoted as ICP.

- **External concentration polarisation (ECP)** occurs in the channels leading to and from the membrane. The reason for ECP is the formation of a boundary layer on each side of the membrane, as the flow is limited very close to the surface of both the support layer and the active layer.

CP is an issue in membranes, since it reduces the osmotic pressure difference leading to reduced permeation. The CP profile is dependent on whether it is used for RO, FO or PRO, and Figure 2.5 illustrates the concentration on the feed and draw sides and inside the membrane and support for PRO.

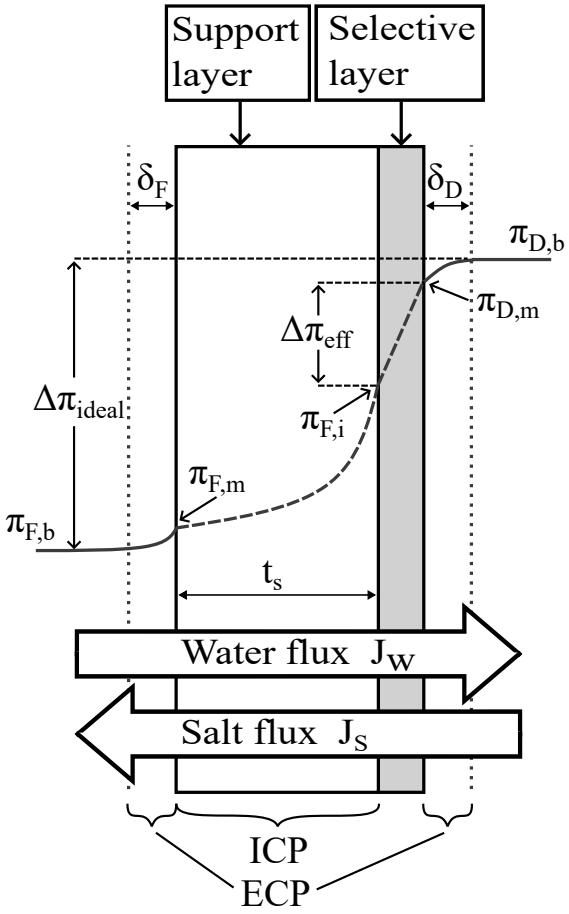

Figure 2.5: Illustration of concentration polarisation over a membrane for PRO. The selective layer denotes the membrane, while the porous support layer denotes the structural support. Figure is inspired by Bhinder et al. (2018).

As can be seen in Figure 2.5, the concentration is low on the outside of the support layer. Due to the formation of a boundary layer, represented by δ_F, the concentration slowly starts to increase. The boundary layer limits mass transportation, leading to ECP in the boundary layer region. Inside the support structure, the rate of increase grows larger closer to the membrane, resulting in ICP. In the selective layer, denoted with grey, the change of concentration is close to linear, while another boundary layer forms on the draw side of the membrane. When calculating the flux over the membrane, it is dependent on the osmotic pressure difference. However, due to ICP inside the support layer and ECP in the boundary layers, the concentration gradient is not equal to the difference between the bulk draw and feed concentrations. Since the concentration gradient is smaller over the membrane, the actual achievable osmotic pressure difference π_{eff} is significantly lower than the total osmotic pressure difference between the feed and the draw

solution, denoted as π_{ideal}. This leads to a reduced flux, relative to if π_{ideal} could be utilised.

As mentioned above, while ICP occurs inside the porous support structure, ECP occurs in the freely flowing fluid and is caused by the boundary layer, as shown in Figure 2.5. Hence, to reduce ECP, more turbulence can be induced in the channel.

The concept of concentration polarisation, as discussed with ICP and ECP, plays a crucial role in an OHE. The OHE capitalises on the difference in osmotic pressure between two solutions, through the use of PRO. The reason for CP being very relevant in OHEs is that the hydraulic pressure over the expander depends on the actual osmotic pressure over the selective layer of the membrane.

2.3 Osmotic Heat Engine

An osmotic heat engine is a thermodynamic cycle that converts chemical energy into mechanical energy. To do this, the principle of PRO is exploited to pressurise the draw solution and thereby drive a turbine. PRO systems are already used for power generation. However, this is usually in coastal areas, where fresh water from rivers meets saline water. By utilising both fresh and saline water, energy can be produced. The technology is also used by the company SaltPower for "solution mining". This means that fresh water is pumped into a salt deposit. The salt then dissolves to saturate the brine, before it is pumped out of the mine to be purified. By passing the brine through a membrane as the draw solution, the pressure of the solution is increased. Doing this and using the pressure increase induced by the membrane to run the pumps, the power that must be supplied to run the brine pumps can be greatly reduced. (SaltPower 2024)
Both of the mentioned uses for the technology utilise an open system, meaning that there is a constant supply of feed and draw solutions. However, another approach is also possible. If heat is added to the system, the feed and draw solutions can be separated after expansion over the turbine. This means that the technology can be used in a closed system configuration.

The open PRO system and the closed OHE system inspired by McGinnis et al. (2007) are illustrated in Figure 2.6 on page 13.

As mentioned above, the open PRO system has constant supply flows of both the feed and draw solutions. The feed solution enters the membrane at ambient pressure, while the draw solution is pressurised using a pressure exchanger (PEX). The draw solution promotes flux over the membrane, and with increased flow the diluted solution is then split between the PEX and a turbine. As the system is open, the energy is harvested through the turbine and the solutions are discarded from the system.

Meanwhile, for the closed OHE system, the working principle is a bit different. The concentration difference over the membrane still promotes permeation, but after the PEX and turbine, the diluted solution is heated up. This evaporates some of the water, leaving a concentrated solution and pure water as steam. The steam is then recycled as feed, while the concentrated solution is resupplied for the draw side of the membrane. Unlike the open PRO system, the OHE needs heat supplied instead of constant draw and feed flows, which could make it viable for waste heat recovery at ultra low temperature regimes ($< 80°C$).

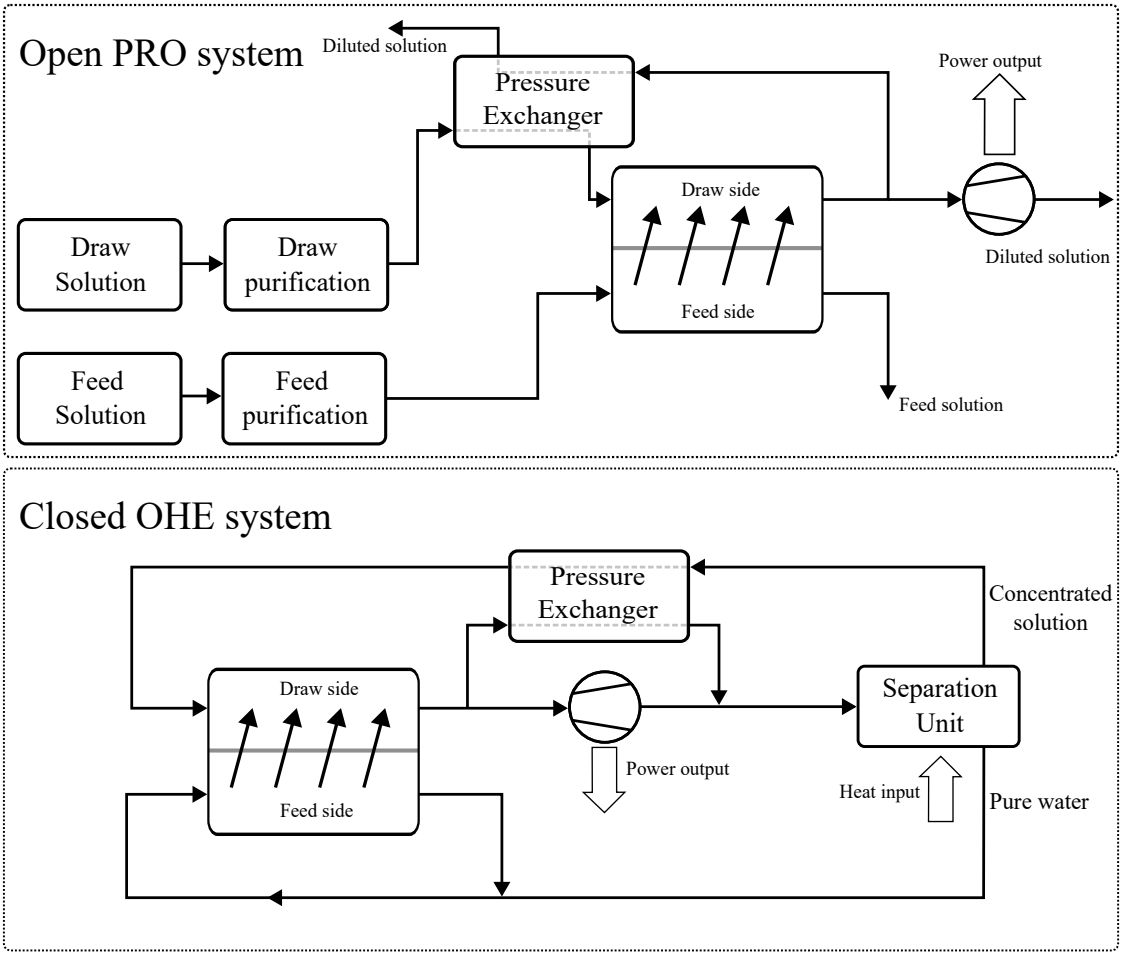

Figure 2.6: Illustration of open system generating power using PRO and a closed system, also known as an OHE, using heat to generate power from a concentration difference. Closed system configuration is inspired by McGinnis et al. (2007).

Chapter 3

Problem Statement

As explained previously, there is a large potential for energy harvesting from low-temperature waste heat harvesting. Several technologies are being researched to accommodate the use of waste heat. One of the technologies proposed is the use of PRO. Although PRO is already being used for energy generation in areas where both fresh water and salt water streams are available, this is done as an open cycle, where the new feed and draw solution constantly flows into the system. For waste heat recovery, the cycle will be closed, leading to the following problem statement:

> *How efficient is a closed-loop osmotic heat engine, using sodium chloride as the solute, to utilise low temperature waste heat and is a sodium chloride based OHE a feasible solution to ultra low temperature waste heat recovery?*

To answer the problem statement and provide further justification for the conclusion, working questions are formulated which aim to improve the understanding of the system.

- What are the main influencing parameters on the performance of the system and which parameters should be in focus to improve the performance of the system?
- What performance parameters should be chosen to evaluate the system?
- Should any changes be made to the closed OHE system proposed in Chapter 2?

Chapter 4

Modelling Approach

In the previous chapter, a problem statement was formulated. To answer this, a model of the system is constructed based on thermodynamics and membrane theory. The following section describes the working principle of the system and how it is coupled.

4.1 System Explanation

The modelled system is a closed cycle PRO system. This means that instead of using a constant stream of salt water, the system is closed such that after the osmotic process, the mixture is separated to be recycled for osmosis. To do this, heat is added to evaporate a desired part of the mixture, making it possible to separate the feed and draw solutions into individual streams. The modelled system is illustrated in Figure 4.1.

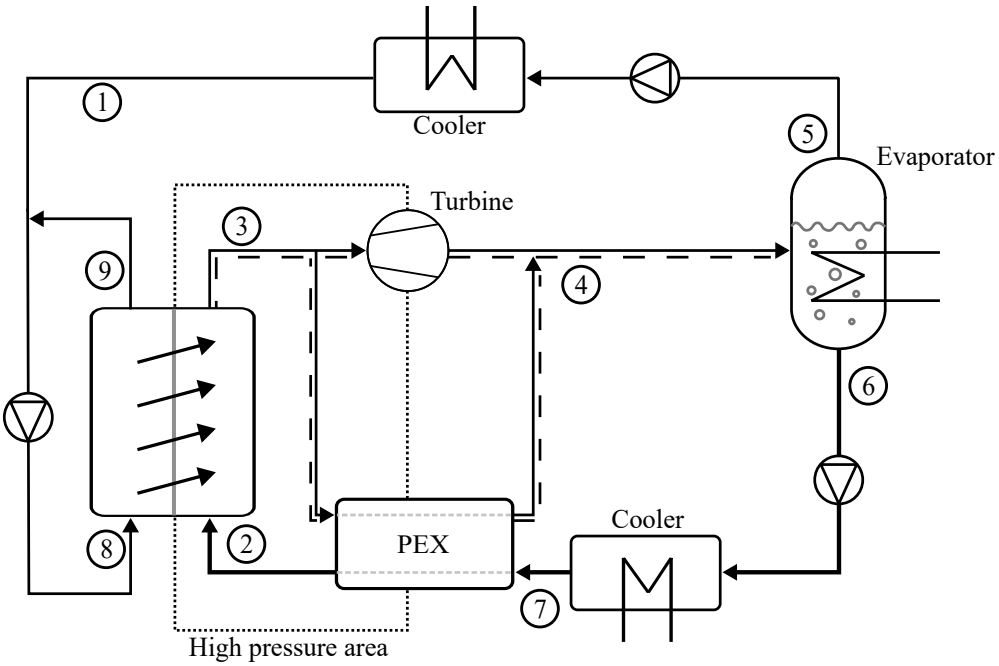

Figure 4.1: Process flow diagram illustrating the OHE system. The thin lines represent water flows, the thin lines with a dashed line besides represent diluted flows and the thick lines represent concentrated flows.

The system consists of a membrane, marked as the dotted line on the left, with the feed solution on the left, and the draw solution on the right. As the osmotic pressure of the draw

solution is higher than that of the feed solution, a high-pressure area is present on the draw side. The diluted draw solution is then pumped into either a hydraulic turbine or a PEX . The splitting ratio is based on how much feed is drawn across the membrane, as the PEX approximately the same amount of flow as is to be pressurised. After the expansion, the flow is then reseparated into the feed and draw solutions through the addition of heat. Afterwards, energy is recovered through cooling, which can be partially used for the heater. The modelling of each component is described in the following section.

4.2 Assumptions

Since the system contains components which are very complex to model accurately, several assumptions are made. The assumptions significantly decrease the simulation time and the complexity of the code, but also come with a cost in terms of accuracy of the model. The assumptions made are described below and are sorted from the one expected to have the most impact to the one with the least impact.

- When salts are used in mixtures, there is a limit to how much can be dissolved. This limit is temperature dependent, so it does not stay constant throughout the system. If the concentrations of the salts are higher than the limit, some of the salt will precipitate as solids. As this is beyond the scope of the project, no precipitation is assumed in the flow. This also results in the assumption that fouling does not occur, which in practice will reduce the performance of the membrane, reducing the flux.
- The density of the salt permeating in the system is assumed to be constant at $1075 \mathrm{kg/m^3}$. This is based on Galamba (2012), but it also means that both the influence of temperature and pressure on the density is assumed to be negligible.
- As the feed and draw solutions diffuse over the membrane, the diffusion coefficient D will change due to the change of concentrations. However, to reduce complexity, the diffusion coefficient is assumed to be constant during the process. As the diffusion coefficient is kept constant, temperature dependence is also assumed to be negligible in this regard.
- It is assumed that there is no pressure loss over the PEX. While this is not realistic, the exact behaviour of the component strongly depends on parameters such as inlet and outlet pressures and viscosity among several other factors. To simplify the modelling of the PEX, the efficiency is expressed only in terms of leakage flow.
- It is assumed that only the water that evaporates leaves as gas from the boiler. This means that no salt particles travel with the steam. Hence, point 5 on Figure 4.1 consists of pure water with no contaminants.
- The system is assumed to be in steady state, meaning that changes to external circumstances, which could alter the operating conditions of the plant, are ignored.
- The model has been designed such that the temperatures of each of the two coolers should be the same. This is because the salt water and the pure water enthalpies are calculated with different models, whose reference states do not align, which severely complicated having different inlet temperatures on each side of the membrane.

4.3 Membrane Model

4.3.1 Theory

Generally, for osmosis, the water flux J_w depends on the membrane properties and is proportional to the osmotic pressure difference over the membrane. The water flux can be calculated by Equation 4.1:

$$J_w = A\Delta\pi \tag{4.1}$$

Where A is the water permeability of the membrane and $\Delta\pi$ is the osmotic pressure difference over the membrane. The water permeability denotes how easily water passes the membrane and is specified in the unit $\mathrm{L}/(\mathrm{m}^2{\cdot}\mathrm{h}\cdot\mathrm{bar})$. When working with PRO, a hydraulic pressure ΔP is applied on the draw side of the membrane. The added hydraulic pressure works against the osmotic pressure difference, reducing the water flux. This is accounted for with Equation 4.2:

$$J_w = A(\pi_D - \pi_F - \Delta P) \tag{4.2}$$

Where π_D and π_F are the osmotic pressures on the draw and feed side of the membrane, respectively. ΔP denotes the hydraulic pressure difference over the membrane. As mentioned in Chapter 2, the available osmotic pressure is not equal to the osmotic pressure of the bulk feed and draw flows. Therefore, ICP and ECP have to be accounted for. To calculate the water flux, accounting for the reduced osmotic pressure difference, Equation 4.3 is proposed. (Kim et al. 2015)

$$J_w = A\left(\frac{\pi_{D,b}\exp\left(-\frac{J_w}{k_D}\right) - \pi_{F,b}\exp\left(\frac{J_w \cdot S}{D}\right)}{1 + \frac{B}{J_w}\left[exp\left(\frac{J_w \cdot S}{D}\right) - exp\left(-\frac{J_w}{k_D}\right)\right]} - \Delta P\right) \tag{4.3}$$

In the equation, B represents membrane salt permeability, which is a measure of how easily salt passes the membrane. $\pi_{D,b}$ and $\pi_{F,b}$ represents the osmotic pressures of the feed and draw bulk solutions, respectively. S denotes the structural parameter for the membrane, which is a measure for the thickness of the support layer, the tortuosity and porosity of the support layer and is calculated through Equation 4.4. (Gonzales et al. 2021)

$$S = \frac{t_s \cdot \tau}{\varepsilon_p} \tag{4.4}$$

Where t_s represents the thickness of the structural layer, τ represents tortuosity, which is the ratio between the shortest possible pathway and the real pathways through the structural layer, while ε_p represents porosity. In Equation 4.3, D denotes the diffusive coefficient for the solute. In the equation, $exp\,(J_w \cdot S/D)$ represents the ICP phenomenon, while $exp\,(-J_w/k_D)$ represents ECP, where k_D is a mass transfer coefficient and is calculated by Equation 4.5:

$$k_D = \frac{Sh \cdot D_s}{d_h} \tag{4.5}$$

With Sh being the Sherwood number, which depends on the Reynolds number Re and the Schmidt number Sc. Sh, Re and Sc can be calculated based on Equations 4.6 through 4.8: (Gonzales et al. 2021)

$$Sh = 1.85 \left(Re \cdot Sc \frac{d_h}{L} \right)^{0.33} \tag{4.6}$$

$$Re = \frac{u_{avg} \cdot d_h}{\nu} \tag{4.7}$$

$$Sc = \frac{\nu}{D} \tag{4.8}$$

For the salt flux, the same approach can be used. However, the salt flux does not depend on the osmotic pressure. Instead, the salt flux equation is based on concentrations on either side of the membrane. The salt flux can be described by Equation 4.9. (Gonzales et al. 2021)

$$J_s = B\Delta C \tag{4.9}$$

As for Equation 4.2, Equation 4.9 does not account for the CP effects in the membrane. Therefore, an expression resembling 4.3 can be defined for salt flux. This is done in Equation 4.10: (Kim et al. 2015)

$$J_s = B \left(\frac{C_{D,b} \exp\left(-\frac{J_w}{k_D}\right) - C_{F,b} \exp\left(-\frac{J_w \cdot S}{D}\right)}{1 + \frac{B}{J_w}\left[exp\left(\frac{J_w \cdot S}{D}\right) - exp\left(-\frac{J_w}{k_D}\right)\right]} \right) \tag{4.10}$$

Where $C_{D,b}$ and $C_{F,b}$ represents the solute concentrations in the feed and draw bulk solutions. It should be noted, that in Equation 4.3, A is multiplied onto the parenthesis, because the water flux is found, while in Equation 4.9, B is multiplied as this equation determines the salt flux.

Based on the water flux, another important parameter was determined by Kim et al. (2015), namely the power density. The power density is a measure of how much energy is produced per unit of membrane area and is a parameter often found in studies researching PRO. The power density is based on the water flux and the applied hydraulic pressure and can be calculated with Equation 4.11.

$$PD = J_w \cdot \Delta P \tag{4.11}$$

The unit for power density is W/m^2. In Figure 4.2, it is illustrated how the hydraulic pressure affects the power power density of the membrane. The dark line illustrates the ideal conditions, meaning that ECP and ICP are not present, while the real curve illustrates how the power density changes, as CP is considered.

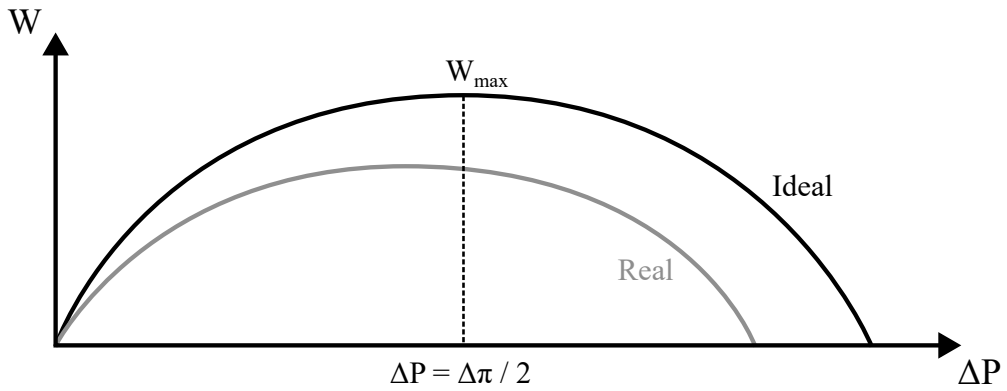

Figure 4.2: Illustration of ideal and real power density as function of the applied hydraulic pressure. Inspired by Gonzales et al. (2021).

As can be seen in Figure 4.2, and as previously stated in Section 1.1, the maximum power density of the membrane under ideal conditions is reached if the applied hydraulic pressure is around half the osmotic pressure difference. Furthermore, it is also clear that under real circumstances, where CP is considered, the reachable power density decreases, and the applied hydraulic pressure to reach the maximum power density is decreased, meaning that $\Delta P < \Delta\pi/2$.

As fluid flows through the hollow fibres and the membrane shell, the pressure decreases due to flow friction. It is expected that this pressure loss is of such significance, that it has to be taken into consideration, due to the pumping work required to compensate for it.

Equation 4.12 can be used to calculate the pressure loss per distance:

$$\frac{dP}{dz} = f\frac{1}{d} \cdot \frac{u^2}{2} \cdot \rho \tag{4.12}$$

Where f represents the friction coefficient. The friction coefficient is dependent on the Reynolds number Re and the ratio between surface roughness and the diameter of the tube.

The friction coefficient equation changes on the basis of whether the flow is laminar. For non-laminar flow $Re > 2300$ is given by the Colebrook equation, and for laminar flow ($Re < 2300$) it is purely dependent on the Reynolds number. Equation 4.13 states the friction factor for laminar flow given that the tube is circular, as is the case with the hollow fibres. Equation 4.14 states the expression for the friction factor for non-laminar flow. (Cengel et al. 2017)

$$f = \frac{64}{Re} \tag{4.13}$$

$$\frac{1}{\sqrt{f}} = -2.0\log\left(\frac{\varepsilon_r/d_{fi}}{3.7} + \frac{2.51}{Re\sqrt{f}}\right) \tag{4.14}$$

In Equation 4.14, ε_r represents the surface roughness. As the friction factor appears on both sides of the Colebrook equation, denoted as Equation 4.14, the expression requires iterating to determine the friction factor. However, Equation 4.15 approximates f with an accuracy of $\pm 2\%$ and does not require iterating to find the solution, hence this expression is used instead. (Cengel et al. 2017)

$$\frac{1}{\sqrt{f}} = -1.8\log\left[\frac{6.9}{Re} + \left(\frac{\varepsilon_r/d_{fi}}{3.7}\right)^{1.11}\right] \tag{4.15}$$

Based on the equations, it is clear that for laminar flows, the friction coefficient is directly proportional to velocity, while this is not the case for turbulent flows.

According to Yoshikawa et al. (1994), the pressure loss for the shell side can be determined with the Kozeny-Carman equation, denoted in Equation 4.16

$$\frac{dP}{dz} = -\frac{2 \cdot k_p \cdot \mu_D}{\pi \cdot \varepsilon_v \cdot r_h^2 \cdot d_s^2} \tag{4.16}$$

Where k_p represents a constant, ε_v represents the void fraction, and r_h is the hydraulic radius of the shell. The coefficient k_p is dependent on the orientation of the fibres and how the shell is packed. For the membrane in question, it is assumed that $k_p = 2$ based on Yoshikawa et al. (1994). The void fraction is a measure of how much of the volume inside the shell is *not* taken up by the fibres. The void fraction can be described by Equation 4.17:

$$\varepsilon_v = 1 - \frac{N_f \cdot d_{fo}^2}{d_s^2} \tag{4.17}$$

The hydraulic radius is a measure for the outer shell, and it can be calculated by Equation 4.18.

$$r_h = \frac{\varepsilon_v \cdot d_s^2}{4 \cdot N_f \cdot d_{fo}} \tag{4.18}$$

Since water and salt permeates through the membrane, concentrations, pressure and mass flow all change based on the distance from the membrane inlet. Therefore, to determine the water and mass permeation over the membrane, the membrane is set up based on a finite difference method (FDM). By doing so, it can be taken into consideration how the continuous change of properties affect the total permeation. The FDM is set up in one dimension for both the feed and the draw side of the membrane. An illustration of the approach can be seen in Figure 4.3, where a single node is illustrated with the dotted lines. Within the node, J_w and J_s represent the water and salt flux for the given node.

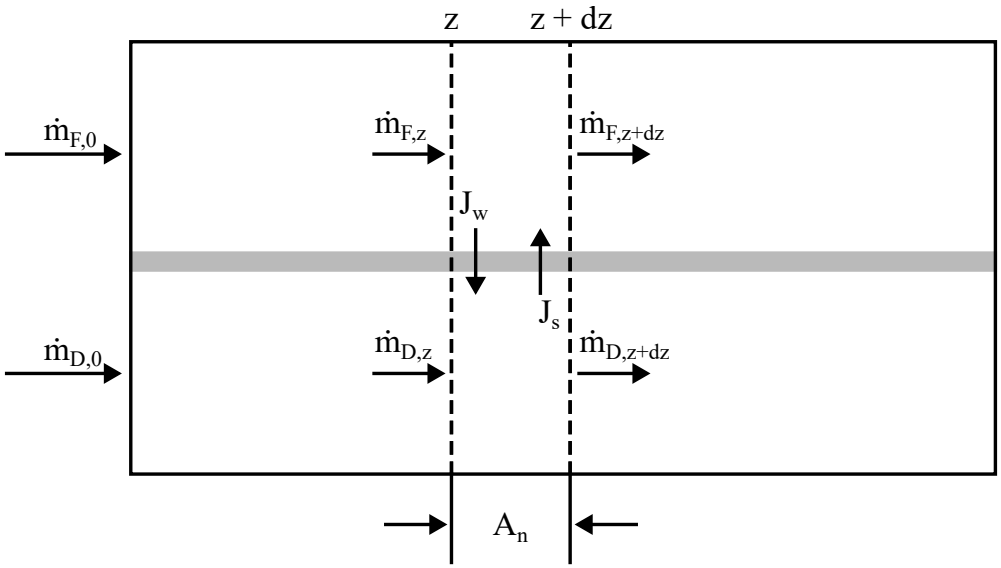

Figure 4.3: Illustration of the FDM used to model the permeation of salt and water over the hollow fibre membrane. Figure is inspired by Geankoplis (2003).

The permeation of water and salt in each node can then be determined based on J_s and J_w with equations 4.19 and 4.20.

$$\frac{d\dot{m}_F}{dz} = (J_s \cdot \rho_\mathrm{s} - J_w \cdot \rho_\mathrm{w}) \cdot A_n \tag{4.19}$$

$$\frac{d\dot{m}_D}{dz} = (J_w \cdot \rho_\mathrm{w} - J_s \cdot \rho_\mathrm{s}) \cdot A_n \tag{4.20}$$

Where A_n denotes the membrane area within the node.

By implementing the described equations in the model, the permeation of water and salt over the membrane can be determined. The implementation is visualised in the flowsheet in Figure 4.4 on page 21. At the start and the end of the flowsheet, the membrane model pulls and returns data to a model of the complete OHE process.

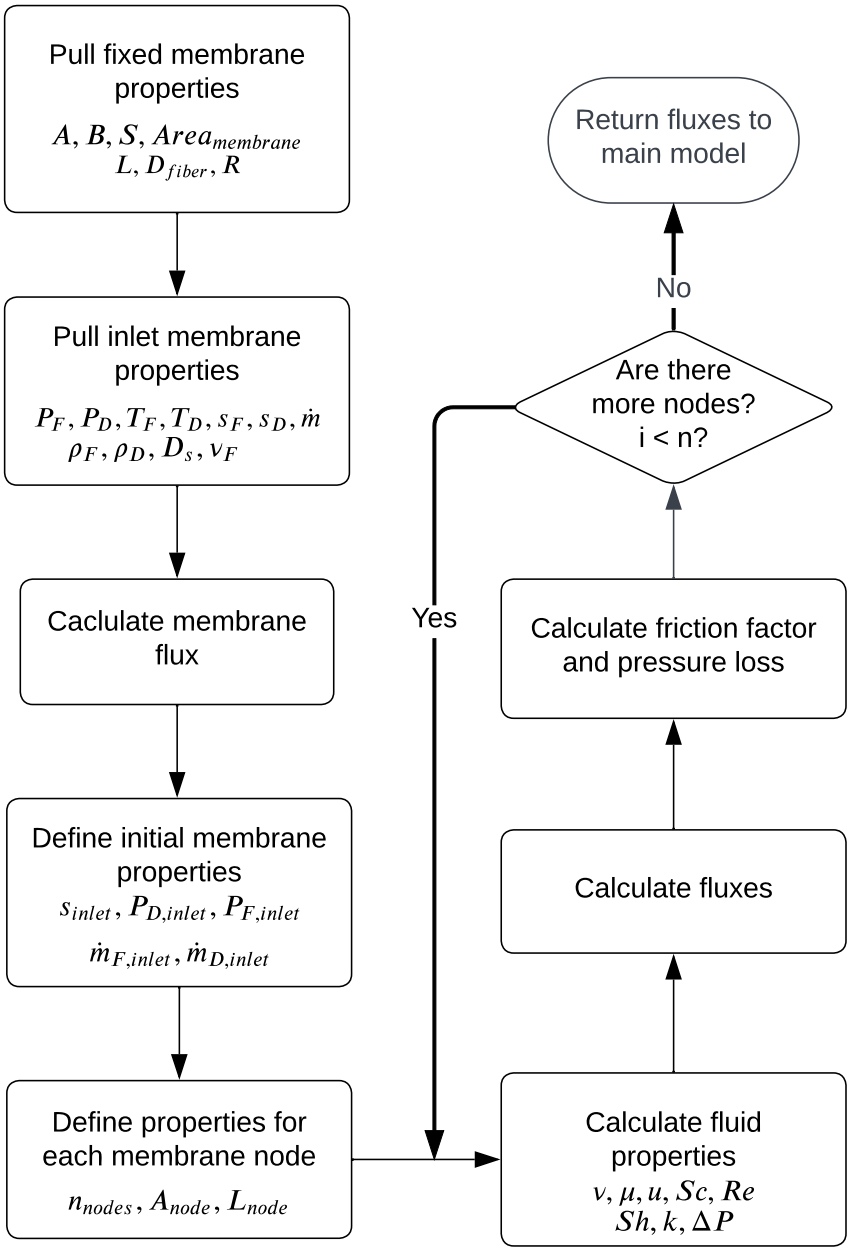

Figure 4.4: Flowsheet describing membrane flux calculation process. The process is part of the full OHE model, which it pulls variables from and returns fluxes, pressures and concentrations to.

The membrane used in the project is, as mentioned, a hollow fibre membrane and is designed for FO. However, the support layer is orientated for PRO as shown in Figure 2.4. The permeabilities and structural parameter for the membrane used in the model are determined by Munubarthi et al. (2020). However, no dimensions of the membrane are stated in the article. Therefore, the membrane parameters are coupled with the dimensions of the membrane as stated from the TOYOBO datasheet in Toyobo (2023a). All the membrane parameters from the article and the datasheet are described in Table 4.1 on page 22 with permeabilities converted from the unit $l/m^2/h$ to $m^3/s/m^2$. Furthermore, of the currently available Toyobo membranes, the one with the highest maximum operating pressure may not exceed 70 bar. (Toyobo 2023b)

Symbol	Definition	Value	Unit
A	Water permeability	$7.5 \cdot 10^{-8}$	$[m^3/s/(m^2 \cdot bar)]$
B	Salt permeability	$9.722 \cdot 10^{-9}$	$[m^3/s/m^2]$
S	Structural parameter	1024	[µm]
L	Membrane length	1.20	[m]
d_{fi}	Inner fibre diameter	$100 \cdot 10^{-6}$	[m]
d_{fo}	Outer fibre diameter	$200 \cdot 10^{-6}$	[m]
d_s	Shell diameter	0.25	[m]
A_m	Membrane area	600	$[m^2]$

Table 4.1: Geometrical and permeate parameters for the membrane used in the project. Data is collected from Munubarthi et al. (2020).

Besides the membrane properties, several other parameters must also be provided to calculate membrane fluxes. The inlet variables of the fluids are listed in Table 4.2. Unless otherwise stated, the membrane parameters used throughout the rest of Chapters 4 and 5 will correspond to the values described in Table 4.1 and Table 4.2.

Symbol	Definition	Value	Unit
$C_{F,0}$	Feed side inlet concentration	0.0	[mol/L]
$C_{D,0}$	Draw side inlet concentration	5.0	[mol/L]
$\dot{m}_{F,0}$	Feed side inlet mass flow	1.5	[kg/s]
$\dot{m}_{D,0}$	Draw side inlet mass flow	0.8	[kg/s]

Table 4.2: Overview of the inlet flow properties for the feed and draw side of the membrane.

Since FDM is used to determine the flux over the membrane, the number of nodes is of great importance for the result of the model. Too few nodes will result in the model being inexact and too many nodes will drastically increase the time needed for the model to finish. To examine the effect of this, a grid convergence analysis is done in Figure 4.5 on page 23, to show the effect of changing the number of nodes.

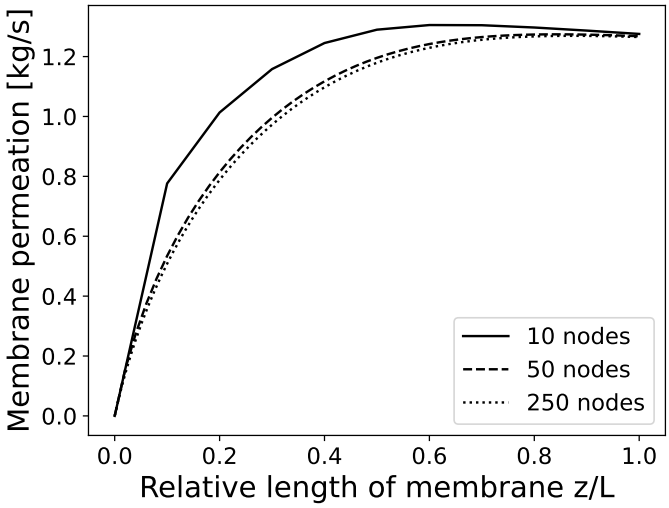

Figure 4.5: Grid convergence analysis of permeation over the membrane as a function of the relative length of the membrane. The permeation is compared for the membrane FDM with 10 nodes, 50 nodes and 250 nodes.

As can be seen, the permeation differs significantly when the number of nodes is changed. To determine how many nodes are required to reach satisfying results, the influence on the total membrane permeation is examined in Figure 4.6.

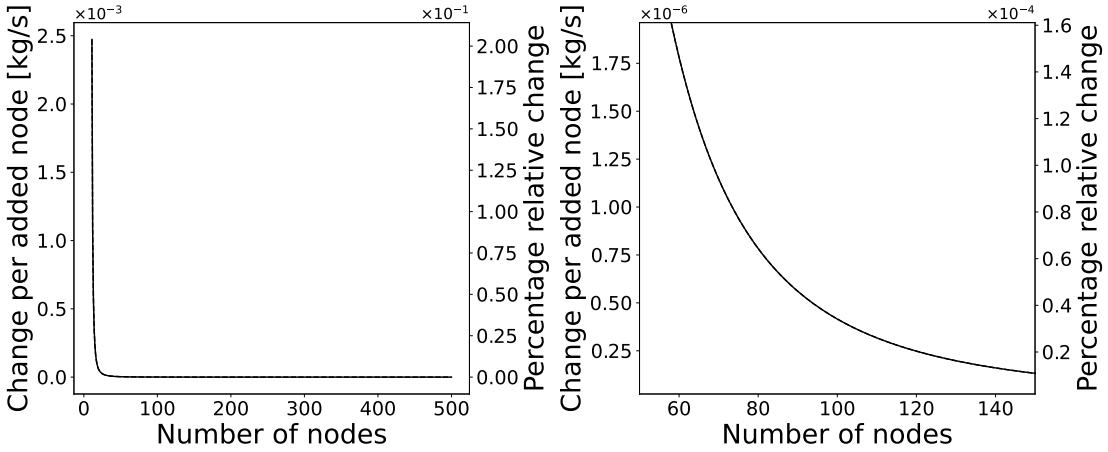

Figure 4.6: Figure describing the change of total permeation per node added to the already existing number of nodes. On the left axis, the absolute change of total permeation. On the right axis, the relative change per added node is described. The right figure displays a zoomed in image of between 60 and 150 nodes.

As illustrated on the figure, the more nodes, the less error is corrected per added node. On the right graph in Figure 4.6, a zoomed image is shown, ranging from 60 nodes to 150 nodes. At 60 nodes, the relative change of adding another node is around 0.0001%, equal to a change of $\approx 1.25 \cdot 10^{-6}$ kg/s which is deemed an acceptable error. But as the parameters are changed to evaluate their effect on the system and the membrane, it is unknown how the accuracy of the FDM model will change. Therefore, to ensure the solution of the FDM model has the desired accuracy, the number of nodes in the model is set to 150. Even though an acceptable error has been determined, the model is yet to be validated with real world data.

4.3.2 Validation of Membrane Model

To validate the model, the ideal solution would be to create an experimental setup and then test a membrane to see if the results of the experiments align with the data yielded by the model. However, due to the limited time available for the project, the validation is done based on experiments published in the literature.

Shibuya et al. (2015) did a study on several membranes, testing them in both AL-FS and AL-DS orientations. For the validation of the membrane model in this project, the AL-DS results will be compared to the model, while the AL-FS results are deemed irrelevant, as these will not be consistent with the results from the model, since the model is based on the AL-DS orientation. The parameters used in the validation are listed in Table 4.3.

Symbol	Definition	Value	Unit
A	Water permeability	$7.389 \cdot 10^{-8}$	$[m^3/m^2/s/bar]$
B	Salt permeability	$2.22 \cdot 10^{-8}$	$[m^3/m^2/s]$
S	Structural parameter	1024	[µm]
L	Membrane length	0.30	[m]
d_{fi}	Inner fibre diameter	$94 \cdot 10^{-6}$	[m]
d_{fo}	Outer fibre diameter	$180 \cdot 10^{-6}$	[m]
A_m	Membrane area	0.12	$[m^2]$
$\dot{m}_F$	Feed inlet mass flow	$5.0 \cdot 10^{-4}$	[kg/s]
$\dot{m}_D$	Draw inlet mass flow	0.01	[kg/s]

Table 4.3: Parameters used for validation of membrane model. Data are collected from Shibuya et al. (2015).

Based on the parameters in Table 4.3, the model is tested for concentrations ranging from 0.3 mol/L to 1 mol/L, with temperatures of 288K, 298K and 308K since this aligns with the experimental data from Shibuya et al. (2015). The water flux from the constructed model in this project, is then compared to the experimentally measured water flux. The results of the model are compared with the experimental data in Figure 4.7 on page 25.

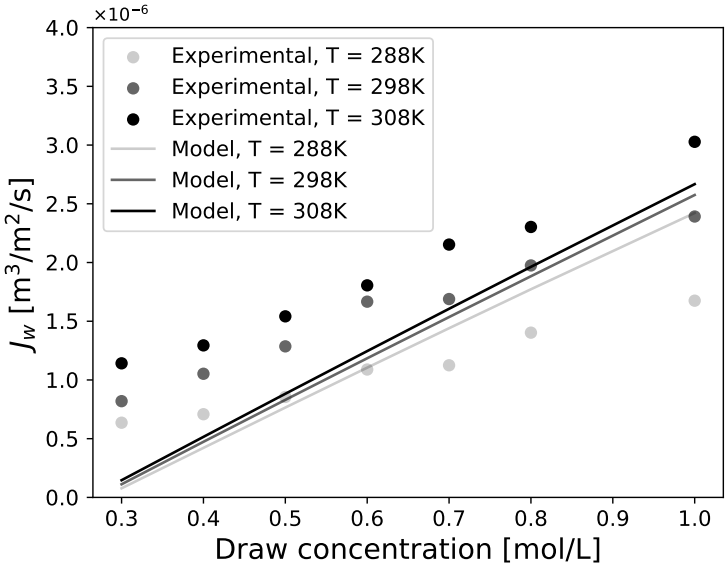

Figure 4.7: Validation of membrane model versus experimental data from literature. Experimental data are collected from Shibuya et al. (2015).

On Figure 4.7, the scattered points represent the experimental data and the lines represent the results of the model formulated throughout this project. Generally, the flux follows the experimental values. However, the modelled flux increases more with concentration than what is the case for the experimental flux. Hence, it seems that the concentration dependence is more significant for the model presented in the project than measured in the experimental data. While inconsistency does appear between the experimental data and the modelling results, the deviations in the validation are expected to be explained by the assumptions made in regards to the temperature dependencies of the system. Furthermore, the diffusivity of the salt is assumed instead of calculated. In Shibuya et al. (2015), the diffusivity is based on the Nernst-Haskell equation. The trends that are shown in the article and the formulated model generally aligns with regard to the behaviour of the flux. It is therefore determined that the validation falls within what is acceptable to trust the model data for the purpose of the project.

Chapter 5

Parametric Analysis of Membrane

As the veracity of the model has been supported, the parameters that affect the results of the membrane model can be analysed. This is crucial to understand how the overall system behaves based on changes occurring due to the way the membrane performs. To examine this, a couple of performance parameters have been determined, which are elaborated in the following section.

5.1 Performance Parameters

To analyse the membrane performance, the main parameters to describe the performance have been determined to be the salt permeation over the membrane, along with the power density of the membrane.

- As the saline water flows on the draw side of the membrane, some of the salt will permeate to the feed side. This will result in an unavoidable increase of feed solute concentration. This reduces the osmotic pressure difference over the membrane, which ultimately reduces the water permeation. Therefore, the extent of this is of large interest.
- To determine the potential for power generation, the power density over the membrane is determined as a performance parameter. Repeating Equation 4.11, the power density can be described as $PD = J_w \cdot \Delta P$ and will be used to evaluate the membrane, since it is a direct measure of how much energy is transferred to the draw solution through permeation.

5.2 Power Density

As previously mentioned in Section 4.3.1, the maximum power density will under ideal conditions be reached when $\Delta P = \Delta\pi/2$, but under real circumstances this is not the case. Therefore, it is of interest to examine how the power density is affected by ΔP. This is done by varying the draw side pressure between the feed side pressure and up to the osmotic pressure of the draw solution. By doing so, the power density can be seen as function of hydraulic pressure difference over the membrane. Furthermore, it is of interest how the concentration affects the power density. This is included by changing the draw side concentration as described in Table 5.1.

Figure 5.1 illustrates the power density as function of the draw concentration and the pressure difference ΔP between the feed and draw sides of the membrane.

Concentration [mol/L]	Osmotic pressure [bar]
1	49.55
2	99.11
3	148.66
4	198.21
5	247.77

Table 5.1: Change of concentration to examine the effects of the concentration on power density.

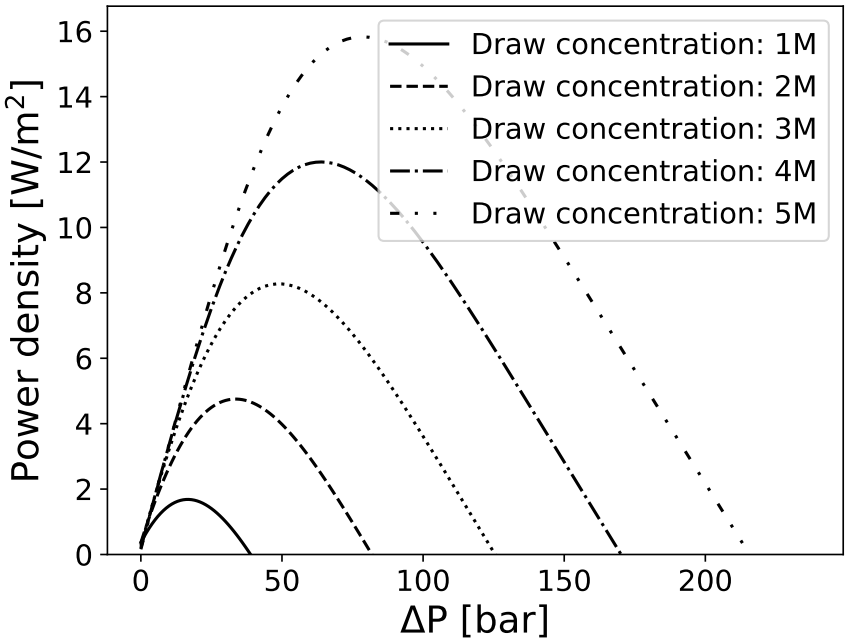

Figure 5.1: Power density over the membrane as function of draw concentration and ΔP.

Based on Figure 5.1, it is clear that the power density is very dependent on concentration. This was also expected because the osmotic pressure, which dictates the flux, is directly proportional to the concentration of the feed and draw solutions. Furthermore, the figure shows that the higher the concentration, the higher ΔP has to be to achieve the maximum power density available. Based on the assumption that the ideal ratio between osmotic pressure difference and applied hydraulic pressure is $\Delta P = \Delta\pi/2$, this seems to make sense. However, the difference between the ideal and real circumstances is greater than expected. For example, for 5M inlet concentration, the expected ΔP would be $\approx$ 120 bar. According to the curve for 5M concentration on Figure 5.1, the modelled maximum power density is reached at $\Delta P = 80$ bar. This can pose both an advantage and a disadvantage, as it means that the mebrane in use does not need to be able to withstand high pressures, but higher pressures also mean that more energy can be harvested in the turbine.

5.3 Permeability and Structural Parameter

When examining how the performance of the membrane is affected by various changes, it is of interest to investigate how the internal parameters of the membrane affect the performance.

When dealing with internal parameters, they can be split into the parameters defined by the support layer and those defined by the active layer. For the active layer, the parameters in question refer to the permeability of water and salt. These have already been covered in the project. As mentioned, the support layer is porous and the purpose of this is to provide structural stability to the active layer. When modelling the fluxes over the membrane, as in Equations 4.3 and 4.10, the structural layer is represented by S, and calculated by Equation 4.4. This means that for the structural layer, only S has to be varied, instead of the tortuosity, the porosity, and the thickness of the layer. The range of variations for each of the parameters is shown in Table 5.2.

Variable	Minimum value	Maximum value	Unit
Water permeability	$3 \cdot 10^{-8}$	$3 \cdot 10^{-7}$	$[m^3/s/m^2]$
Salt permeability	$3 \cdot 10^{-8}$	$3 \cdot 10^{-7}$	$[m^3/s/m^2]$
Structural parameter	200	2000	[µm]

Table 5.2: Variation interval of water permeability, salt permeability and structural parameter.

Based on the variables described in Table 5.2, the power density and salt permeation are examined in Figure 5.2. The figure on the left shows the power density in W/m^2 and the figure on the right shows the salt permeation from the draw to the feed side in kg/s.

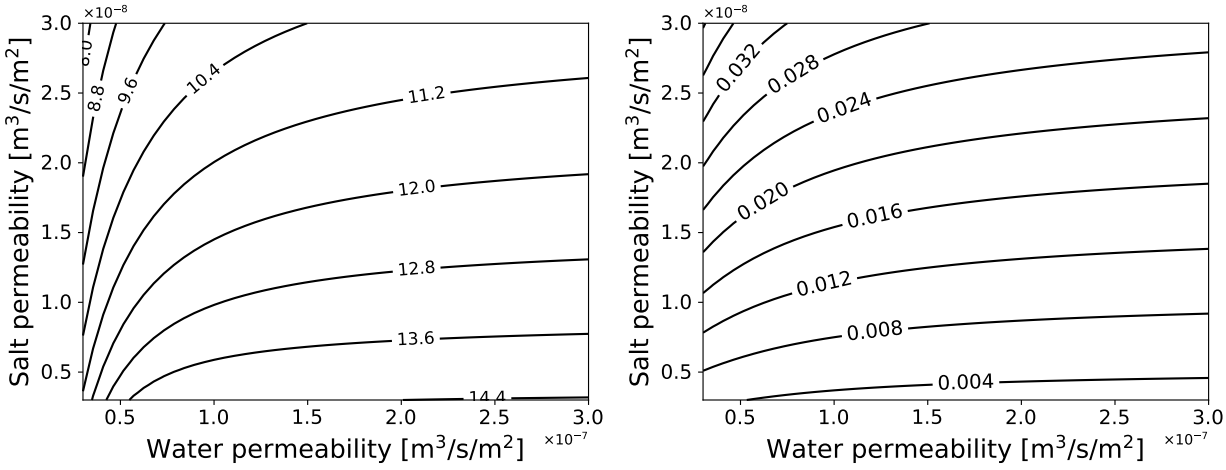

Figure 5.2: The left graph illustrates the membrane power density in W/m^2. The right graph illustrates the salt permeation over the membrane in kg/s as function of water and salt permeability.

Based on the left graph in Figure 5.2, it is clear that the highest power density is reached by making the A/B ratio as high as possible. It does however seem like the power density is less affected by A, the lower the value of B, which suggests that power density gains mainly arise from reducing B even though high A/B ratios must be maintained to give the highest power density. The figure on the right shows the same tendency for salt permeation. Hence, increasing the A/B ratio seems to increase the power density, while the salt permeation decreases. This

suggests that the higher the A/B ratio, the better suited the membrane is for PRO.

When analysing the internals of the membrane, the structural parameter also plays a role. Figure 5.3 shows the effects on the power density as the structural parameter is varied within the interval shown in Table 5.2.

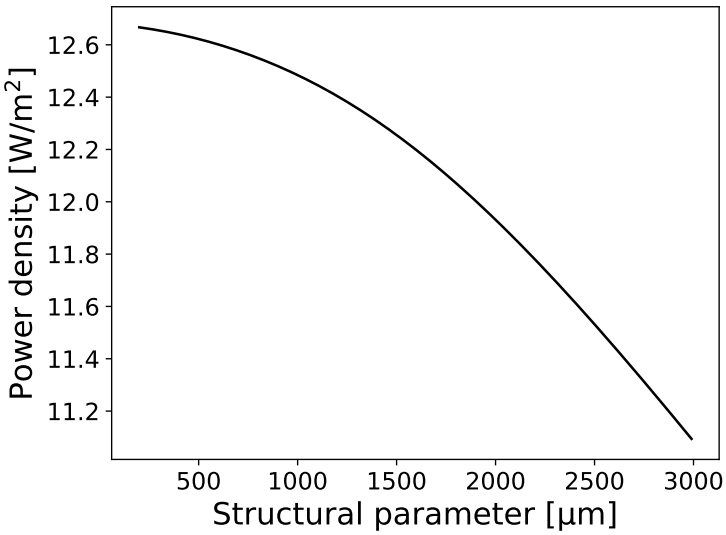

Figure 5.3: Graph representing the change of power density as function of varying the structural parameter S between 200µm and 2000µm.

Figure 5.3 shows that an increase to the structural parameter reduces the membrane power density. Equation 5.1 restates equation 4.4, and when considering that the structural parameter is directly proportional to the thickness of the support layer and the tortuosity of this, as well as inversely proportional to the porosity of the support layer, it is expected that an increase in the structural parameter reduces the power density.

$$S = \frac{t_s \cdot \tau}{\varepsilon_p} \tag{5.1}$$

While increasing the structural parameters does indeed decrease the power density, it should be noted that the effect of doing so is less significant than what was the case for the permeabilities found in Figure 5.2. In this regard, salt permeation is also of interest, which is shown in Figure 5.4 on page 30.

As can be seen in Figure 5.4, salt permeation decreases as the structural parameter increases. This would be expected, as the increase to structural should affect both the salt flux and the water flux. However, it is clear that the dependency is much weaker than for the power density. While lower salt permeation generally would be desirable, this is the same tendency as was shown for the power density and therefore further strengthens the theory that increasing the structural parameter has a negative effect on the overall permeation over the membrane.

Now that the internal parameters of the membrane have been covered, several external parameters are also expected to affect the membrane performance. Generally, the external parameters in focus are related to the inlet conditions of the flow into the membrane. These are covered in the following sections.

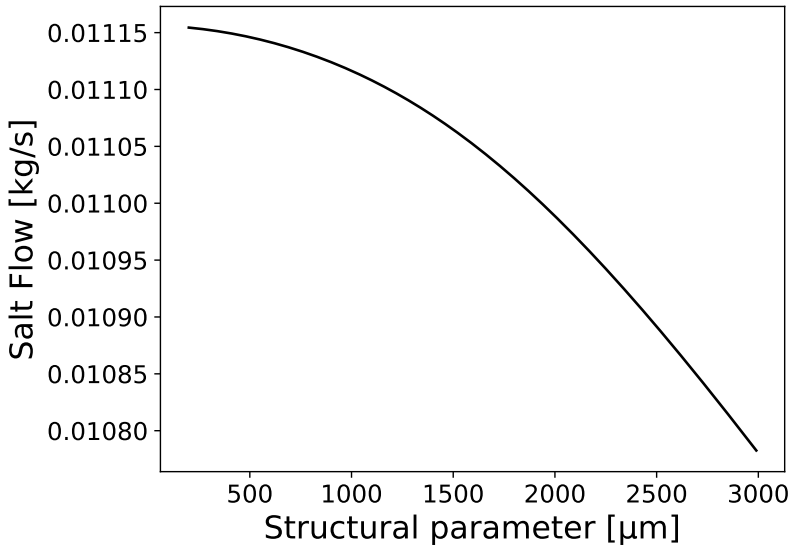

Figure 5.4: Graph representing the change of salt permeation as function of varying the structural parameter S between 200µm and 2000µm.

5.4 Mass Flow Rates

When discussing external parameters, inlet flow rates are expected to have a large effect on the performance of the membrane. To examine the effect of these, they are varied on both the feed and draw side of the membrane in the intervals listed in Table 5.3.

Variable	Minimum value	Maximum value	Unit
Inlet feed mass flow	0.25	2.5	[kg/s]
Inlet draw mass flow	0.5	2.75	[kg/s]

Table 5.3: Variation interval of feed and draw inlet mass flow rates into the membrane.

Figure 5.5 shows the results of varying the inlet mass flow rates in the intervals of Table 5.3. The graph on the left describes the power density in W/m^2 while the figure on the right describes the salt permeation over the membrane in kg/s.

Figure 5.5 on page 31 shows that an increase in both the feed and mass flow rates has a positive impact on the power density. This was also expected since the mass flow rates should be related to the mass transfer coefficients for both the feed and draw side of the membrane. As stated in Section 4.3.1, the mass transfer coefficient is included in the calculation of the ECP phenomenon, which means the occurence of ECP is inversely related to the mass transfer coefficient. While the inlet mass flow rates seems to show a positive effect on the power density, an increase to salt permeation also occurs, as can be seen in the figure on the right. This is an undesired consequence and furthermore, an increase in mass flow rates also results in an increase of flow velocities which increases the pressure loss, as stated by Equation 4.12. Therefore, very high mass flows will not necessarily be a good solution, as it increases the work needed to pump the fluid through the membrane.

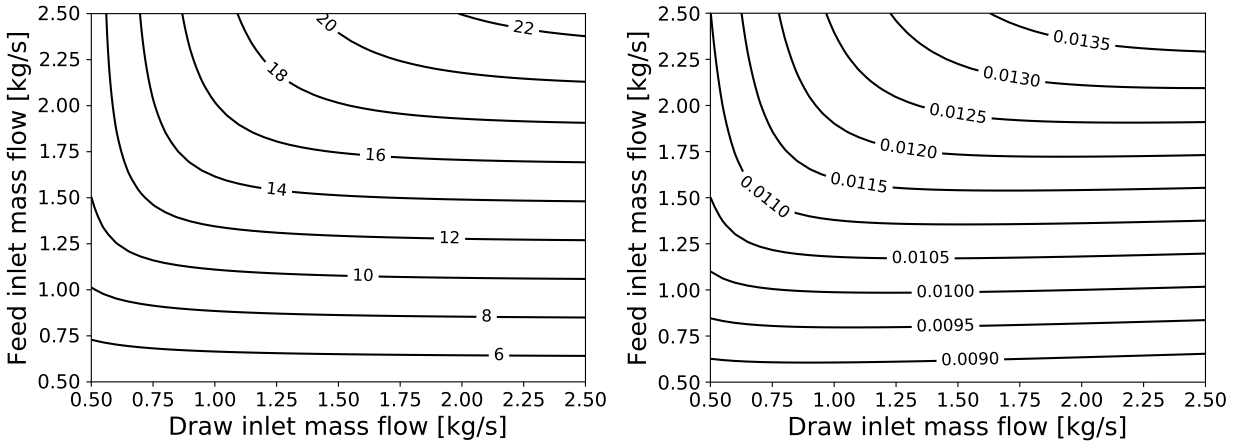

Figure 5.5: The left graph illustrates the membrane power density in W/m^2 as function of inlet mass flow rates into the membrane for both the feed and draw side. The right graph illustrates the salt permeation over the membrane in kg/s.

5.5 Concentrations

The driving force for osmosis is a concentration gradient. Therefore, the inlet concentrations on both side of the membrane are expected to be of significant importance. To verify whether this is the case, the inlet concentrations on the feed and draw side of the membrane are varied in the intervals listed in Table 5.4

Variable	Minimum value	Maximum value	Unit
Inlet feed concentration	0	1	[mol/L]
Inlet draw concentration	1	5	[mol/L]

Table 5.4: Variation interval of feed and draw inlet mass flow rates into the membrane.

As seen in Table 5.4, the feed interval limits are lower than the draw interval limits. This is because it is not of interest to examine situations where the feed inlet concentration is higher than the draw inlet concentrations, since this would yield permeation in the opposite, and undesired, direction. Figure 5.6 on page 32 shows the results of varying the concentrations in the intervals described in Table 5.4.

As expected, Figure 5.6 shows that the concentration dependence is very strong. It even seems that for low concentration differences, the power density becomes negative. This is likely due to the fact that at very low osmotic pressure differences, the hydraulic pressure is larger than the osmotic pressure difference, which will result in a negative water flux. From the right graph, it can be seen that for higher concentration differences, the salt permeation also increases. This makes sense since the salt flux is directly dependent on the concentrations on each side of the membrane. Even though high concentration differences yield a high power density, it is a tradeoff, since the salt permeation also increases, which is undesirable. Furthermore, a natural limit persists with regards to concentration. This is because the salt will begin to permeate if the concentration becomes too high, as can be seen in Figure 2.2 on page 8. To allow for lower concentration differences over the membrane, the hydraulic pressure can be reduced, which is also examined in the following section.

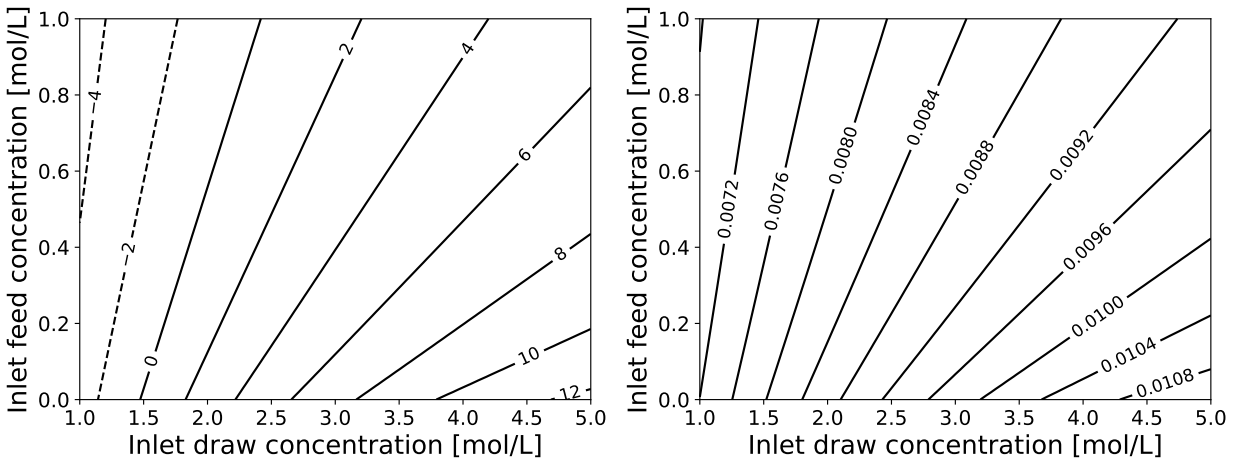

Figure 5.6: The left graph illustrates the membrane power density in W/m^2 as function of inlet concentrations into the membrane for both the feed and draw side. The right graph illustrates the salt permeation over the membrane in kg/s.

5.6 Pressures

As stated, the hydraulic pressure is very important in relation to the inlet concentrations for the membrane. While a lower hydraulic pressure will permit a lower concentration difference, it is expected that it will also decrease the power density over the membrane, reducing the energy available to harvest in the turbine.

The examined intervals for the inlet pressure on the feed and draw side of the membrane are described in Table 5.5.

Variable	Minimum value	Maximum value	Unit
Inlet feed pressure	5	15	[bar]
Inlet draw pressure	20	70	[bar]

Table 5.5: Variation interval of feed and draw inlet mass flow rates into the membrane.

In Section 5.2, it was mentioned that the maximum power density was found at an applied hydraulic pressure difference of around 80 bar for a 5M concentration difference. As shown in Table 5.5, the minimum feed pressure is set to 5 bar. By not letting the feed pressure go low, the stability of the model is ensured. Since the maximum allowable pressure for the membrane is 70 bar, this is set as the maximum pressure for the draw side of the membrane, meaning that the maximum examined hydraulic pressure difference is 65 bar. The results of the variation are shown in Figure 5.7 on page 33.

As expected, Figure 5.7 shows that the power density increases with hydraulic pressure and so does the salt permeation. The increase in power density relative to hydraulic pressure seems to be close to linear until around 60 bar of hydraulic pressure. This aligns well with Figure 5.2 for the 5M concentration, which showed the same trend. The salt permeation increases along with the power density, which means that while more power can be drawn from the system through the turbine with increased pressure difference, the increased salt permeation might have effects, which have to be considered.

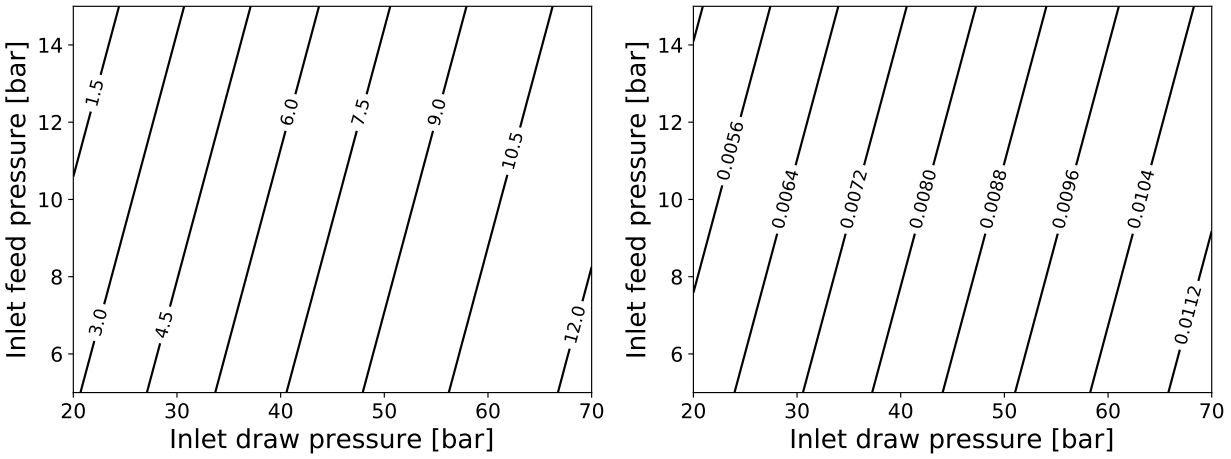

Figure 5.7: The left graph illustrates the membrane power density in W/m^2 as function of inlet pressure variations into the membrane for both the feed and draw side. The right graph illustrates the salt permeation over the membrane in kg/s.

5.7 Key Takeaways for Membrane Performance

In this chapter, the effect on membrane performance from several different parameters has been examined. As expected, most of the parameters examined have a significant effect. In regards to membrane permeabilities and the structural parameter, it is obvious that choosing the right membrane for the purpose is crucial for good performance. In regards to the external parameters (inlet flow rates, pressure and concentrations), they should all be considered, however the mass flow does seem to have the most significant effect. As expected the system performs better, the larger the concentration and pressure differences over the membrane. As the mass flows are increased, it was also expected that the power density would follow. Then, as the mass flows would grow large enough, the power density would once again begin to decrease, as the internal pressure on each side of the membrane would decrease. It turned out that this did not happen, as the power density instead continued to increase with the mass flows and no peak seemed to appear.

Based on the examined parameters in this chapter, a better understanding of how the membrane performance is affected by both the internal and external factors. It is however not certain, that each property has the same effect when analysing on a system level for the whole OHE system, which is yet to be analysed. The framework for doing so is described in the following chapter.

Chapter 6

Modelling the OHE

6.1 Implementation of Bypass Stream

As shown in Chapter 5, some salt permeates over the membrane from the draw to the feed side. This permeation is shown in Figure 6.1 as function of the relative membrane length. The model is based on the data described in Tables 4.1 and 4.2.

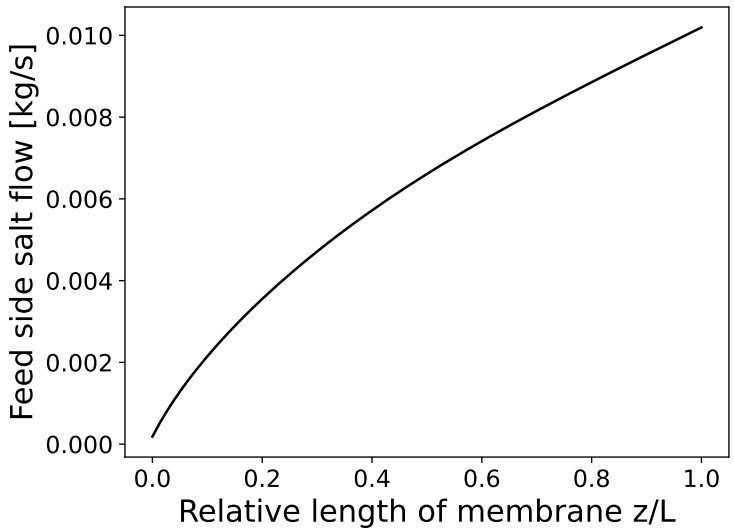

Figure 6.1: Graph illustrating the development of the salt flow of the feed side of the membrane for a single pass over the membrane. The membrane is modelled based on data from Tables 4.1 and 4.2.

As can be seen in Figure 6.1, one pass over the membrane increases the amount of salt flowing on the feed side of the membrane from zero to around 0.01 kg/s. In the system proposed in Figure 4.1, feed water is continuously supplied from the evaporator, but the salt that permeates through the membrane to the feed side is not removed. Because of this, the salt accumulates on the feed side of the membrane, and would continue to do so until the concentrations are equal. To examine the extent to which this affects the water permeation, a model is constructed of the membrane with the solution leaving through the outlet of the feed side is then recirculated back to the inlet of the membrane. For every pass over the membrane, extra water is added, so that the total inlet mass flow remains constant, and the new salinity of the feed solution is calculated based on the ratio between the recirculated solution and the added pure water. The setup for the model is illustrated in Figure 6.2 on page 35.

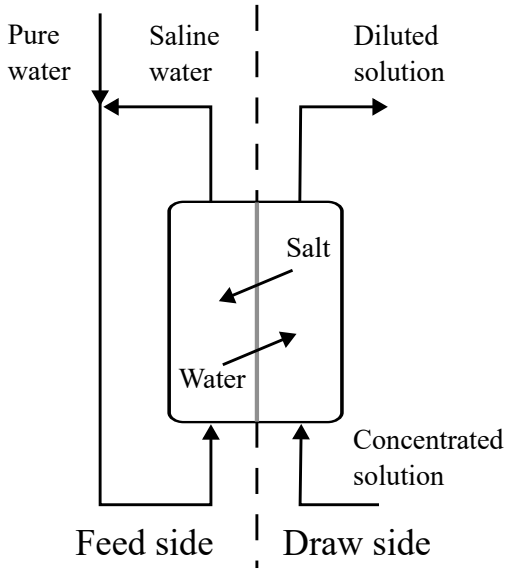

Figure 6.2: Illustration of the model setup to examine the effect of salt accumulation on the feed side of the membrane with no bypass stream to the draw side. The left side is the feed side of the membrane, while the right side is the draw side. The arrows denote the direction of water and salt permeation.

Based on the illustrated setup and the data in Tables 4.1 and 4.2, Figure 6.3 shows the development of water permeation as function of the salinity in the solution for each pass through the membrane.

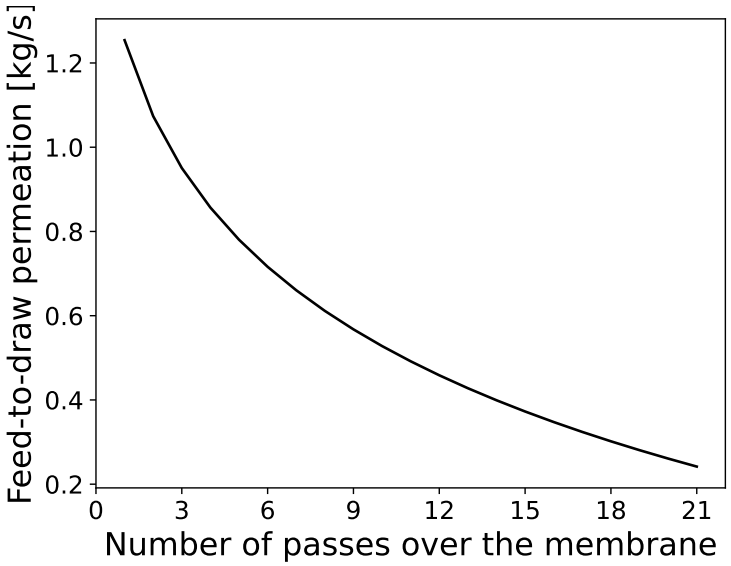

Figure 6.3: The effect of salt accumulation on the water permeation from feed to draw side of membrane. The effect is due to recirculation of the solution leaving the feed side of the membrane as shown in Figure 6.2.

Figure 6.3 shows a clear and significant decrease in permeation for each pass over the membrane. This is as expected, as the increase in concentration in the feed solution directly reduces the osmotic pressure difference over the membrane and therefore is directly proportional to a reduction of the water flux. This is also described by Equation 4.3. To overcome the arising issues from salt permeation, some of the feed solution is bypassed to the draw side of the membrane, just after the expansion. By doing so, some of the salt is removed from the feed side of

the membrane, forming an equilibrium in salt concentration, which will invevitably be lower than the draw side concentration. In this project, the bypass stream is implemented as shown with the grey dotted arrow in Figure 6.4.

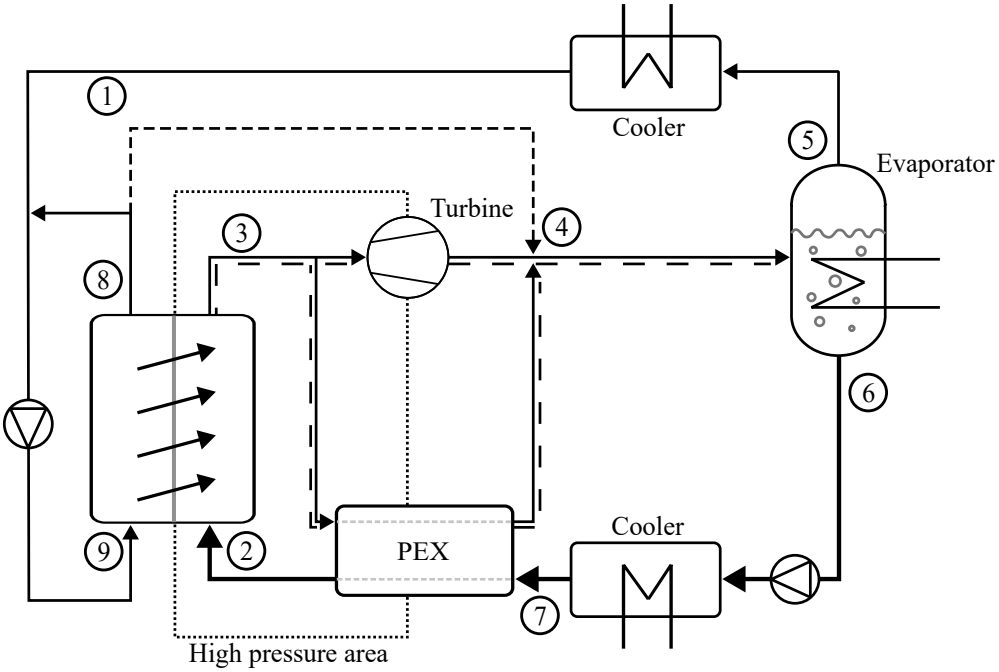

Figure 6.4: Process flow diagram of the OHE with a bypass stream implemented. The thin lines represent water flows, the thin lines with a dashed line besides represent diluted flows and the thick lines represent concentrated flows.The bypass stream is represented by the single dashed line going from point 8 to point 4.

6.2 System Components

The system shown in Figure 6.4 contains several components that manipulate the fluid flow and the energy content of these. Therefore, the following section describes the modelling approach to include the effects of each component.

Pressure Exchanger

A pressure exchanger (PEX) is an energy recovery device that works by recouping the pressure energy from a high pressure stream to a low pressure stream. The PEX used in this project is a so called rotary PEX device, which is built up from two plates with a rotor between these. The PEX might have a pump and motor, but these are only required to make up for energy lost in the PEX device as the component is not isentropic. An illustration of the working principle of a PEX is shown in Figure 6.5 on page 37.

On Figure 6.5, the low and high pressure inlet and outlets, are located in the end plates. Between the end plates is a rotor with pipes running through, as can be seen in the figure. The PEX is installed such that the pressure in both ends of the pipe is the same. Fluid will be pumped in from the inlet pipe, which displaces the fluid already present and pushes this into the outlet pipe in the opposite end plate. By rotating the rotor, this means that the fluid entering at low pressure is now leaving at high pressure and opposite. Generally, a PEX device can be a good solution to increase the system efficiency, as the PEX transfers the pressure energy at

Figure 6.5: Illustration of PEX working principle. The dotted box illustrates the rotor and the fluid balances inside this, while the left and right side denotes the inlets through the end plates.

an efficiency which can be greater than 95%. (Energy Recovery 2024) The efficiency of a PEX device is defined by the energy leaving the component, divided with the energy that enters, as described in Equation 6.1.

$$\eta_{PEX} = \frac{(\dot{m}_{HP} - \dot{m}_L) \cdot P_{HP} + (\dot{m}_{HP} + \dot{m}_L) \cdot P_{LP}}{\dot{m}_{HP} \cdot P_{HP} + \dot{m}_{LP} \cdot P_{LP}} \tag{6.1}$$

In reality, the pressure of the fluid coming out on the high-pressure side would be lower than the pressure entering, which would result in enthalpy loss along with the leakage flow. This would be accomodated by a small pump connected to the PEX. To simplify the model, it is assumed that the pressure coming out of the PEX is equal to the pressure entering. To accommodate for this, the leakage flow is calculated based on 5% enthalpy loss, instead of the leakage flow of 1- 2% that would normally persist in a PEX unit. (Stover 2005) Based on this, the leakage flow can be determined as 6.2.

$$\dot{m}_L = \frac{(\eta_{PEX} - 1)\,(\dot{m}_{HP} \cdot P_{HP} + \dot{m}_{LP} \cdot P_{LP})}{-P_{LP} + \dot{m}_{HP}} \tag{6.2}$$

To achieve a better understanding of the working principles of a PEX device, it is advised to watch the animation made by the company Energy Recovery in Energy Recovery (2020).

Turbine

The turbine in the system is used to convert the kinetic energy added by the membrane into electrical energy. The energy balance for an isentropic turbine can be denoted based on the work drawn work, the mass flow rate and the enthalpies as described in Equation 6.3.

$$\dot{m}_{turb} \cdot h_{in} = \dot{m}_{turb} \cdot h_{out} + W \tag{6.3}$$

Where $\dot{m}_{turb}$ represents the mass flow through the turbine, h_{in} and h_{out} are the enthalpies of the fluid entering and leaving the turbine, respectively and W represents the work extracted from the turbine. In reality, turbines are not isentropic, hence the turbine efficiency must be accounted for in the equation. To calculate the power output from the turbine, Equation 6.3 can be rewritten as Equation 6.4:

$$P_{turb} = \eta_{turb} \cdot \dot{m}_{turb} \cdot (h_{in} - h_{out}) \tag{6.4}$$

Where η_{turb} denotes the total efficiency of the turbine, which is set to 0.9 in the project. This is achievable for a Pelton turbine which is well suited for hydraulic pressures in the range of this project. (Dixon and Hall 2014)

Pump

The system uses pumps to circulate the fluids around the system and to achieve the desired split flows into the PEX. The pumps used in the system are peristaltic pumps, which is a type of positive displacement pump that uses a flexible tube such that the fluid is only in contact with the tube, thereby preventing any form of contamination of the fluid. A peristaltic pump is illustrated in Figure 6.6.

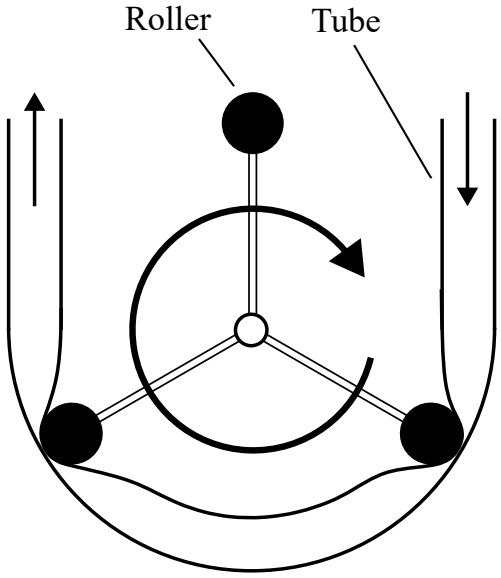

Figure 6.6: Illustration of a peristaltic pump. The rotating motion of the roller shuts off the pipe, forcing the fluid forward.

The peristaltic pump illustrated in Figure 6.6, works by compressing the tube. By doing so, the tube becomes sealed on both sides of the fluid, which forms a pocket. Work is added to the fluid by the rotation of the rollers, pushing the fluid to the high pressure side of the pump. The energy balance for the pumps can be calculated by Equation 6.5.

$$\dot{m} \cdot h_{out} = \dot{m} \cdot h_{in} + W \tag{6.5}$$

where W is the energy added to the fluid by the pump. To calculate the necessary pumping power that must be supplied, the efficiency is multiplied by the added work, as calculated in Equation 6.6.

$$P_{pump} = W \cdot \eta_{pump} \tag{6.6}$$

In the model, the total pump efficiency is set to $\eta_{pump} = 0.8$. This is an assumption, as a source stating the efficiency of peristaltic pumps has not been found. DXP Pacific (2023) does however state that peristaltic pumps generally are more energy efficient than centrifugal pumps.

Heat exchanger

The heat exchangers are used to cool the fluids after the boiler. The energy balance of the heat exchanger is dependent on the inlet and outlet enthalpies, as well as the mass flow. When working with heat exchangers, pressure loss is necessary for proper cooling. This is because pressure loss indicates turbulence which promotes heat exchange. The higher the pressure loss the more efficient the heat transfer will become, of course assuming that the exchanger is well designed. To account for this, the pressure loss in each exchanger is assumed to be 1 bar. As the enthalpy denotes the energy flow into and out of the heat exchanger, the energy balance can be defined with Equation 6.7.

$$\dot{m}_{HEX} \cdot h_{out} = \dot{m}_{HEX} \cdot h_{in} \tag{6.7}$$

Separation

Before recirculating the fluid back to the membrane, the feed solution must be regenerated. To do this, the solution is heated to evaporate water from the concentration, thereby concentrating the draw solution and yielding a pure water flow for the feed side of the membrane. This is also shown in Figure 6.7.

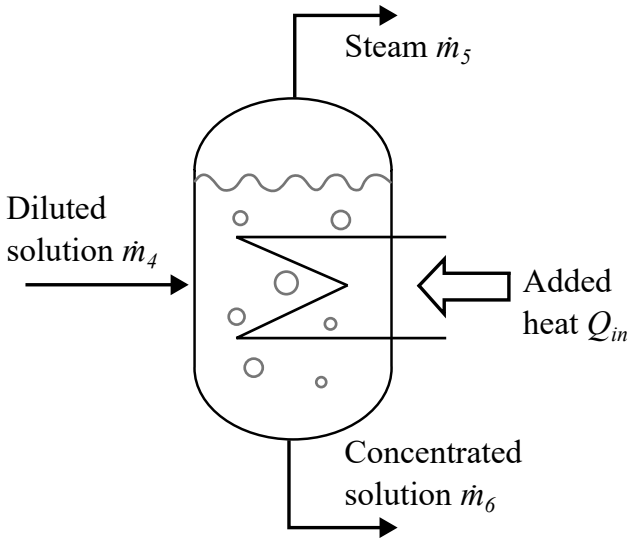

Figure 6.7: Illustration of the separation process used in the modelled OHE. The mixture enters the separator after the turbine and pure steam is generated to be supplied to the feed side of the membrane.

To model the separation, several unknown variables must be determined. For the separation process, stream 4 while stream 5 and 6 leaves. The flow rate of streams 5 and 6 and the salinity of stream 6 must be determined. This means that there are three equations to be solved. Stream 5 is based on evaporation of the salt water, so it is assumed no salt molecules travel to this stream. This leaves three unknown factors, $\dot{m}_5$, $\dot{m}_6$ and $x_{s,6}$ which denotes the mass fraction of salt in this stream. While the mass fraction is dimensionless, it can be interpreted as having the unit kg salt / kg water, so the salinity can be determined as $s_6 = x_{s,6} \cdot 1000\text{g/kg}$.

The first equation necessary, is Equation 6.8. It represents a mass balance and ensures that the mass which enters the boiler, is equal to the total mass leaving.

$$\dot{m}_4 = \dot{m}_5 + \dot{m}_6 \tag{6.8}$$

Equation 6.9 is a mass balance for the salt content of the streams entering and leaving the separation process. Since it is assumed that no salt molecules leaves the separator with the evaporated water, the salt balance is based on the mass flows and mass fraction of streams 4 and 6.

$$x_{s,6} \cdot \dot{m}_6 = x_{s,4} \cdot \dot{m}_4 \tag{6.9}$$

This expression is isolated to determine the mass fraction of salt in stream 6, resulting in Equation 6.10:

$$x_{s,6} = \frac{x_{s,4} \cdot \dot{m}_4}{\dot{m}_6} \tag{6.10}$$

The last equation for the separation determines the amount of water evaporated. As the pure water is led to the membrane, the mass flow over the membrane must equal the mass flow in stream 5. Equation 6.11 ensures defines the mass balance for relation:

$$\dot{m}_{membrane} = \dot{m}_5 \tag{6.11}$$

By combining the components, a model of the system can be constructed. The methodology behind this is described in the following section.

6.3 Modelling approach

Since the OHE is a closed system, the output of each of the components affects the input of the same component. Hence, to find a solution, it is necessary to iterate the system. The model to do so can be split into the following processes:

- Initiation, where the fixed system parameters are defined
- Definition of membrane inlet properties
- Calculation of water and salt flux over the membrane, calculated through a finite difference approach.
- Updating streams and salt concentrations throughout the system

This approach continues, until the system is converged, to calculate the efficiency of the system afterwards. The approach described above is also visualised through a flow sheet in Figure 6.8 on page 41.

Based on the proposed methodology, the following chapter explores the use of the OHE through a parametric study to examine the effects on the system as the working conditions of the system are changed.

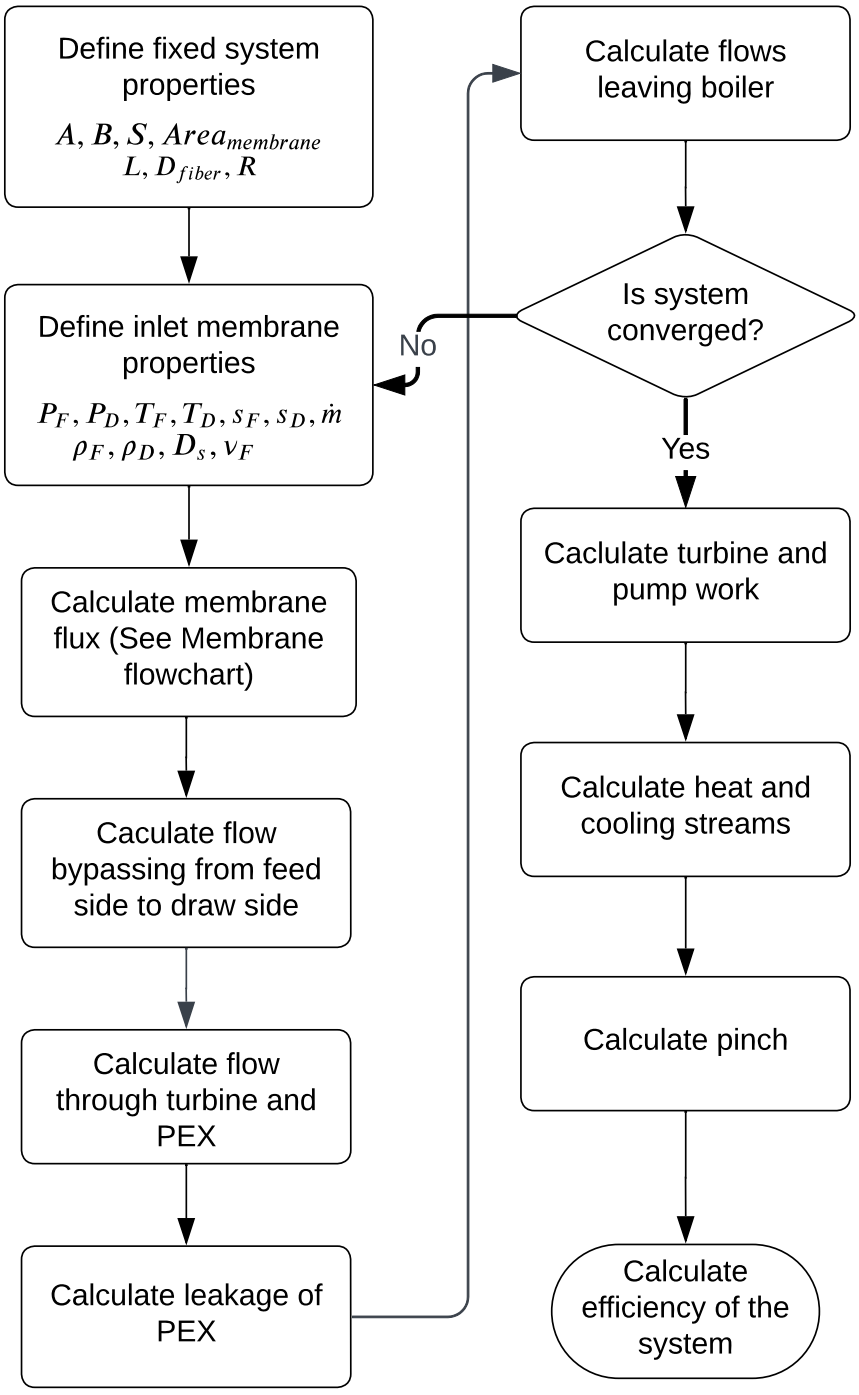

Figure 6.8: Flow sheet describing the modelling approach of the system

Chapter 7

Parametric Analysis of OHE

Now that the membrane process has been explained and modelled in Chapters 4 and 5, respectively, the focus shifts to the OHE as a whole system. The aim of this analysis is to determine the efficiency of the system and hopefully to identify areas available for improvement. This is both from a parametric focus and if the system should be redesigned to achieve better performance.

7.1 Performance Parameters

The objective of this part of the project is to understand and improve the efficiency of the entire OHE system. To do so, a set performance parameters is identified, as these are believed to be well representative for the performance of the entire system. The chosen performance parameters are the coefficient of performance (COP) and the total efficiency. The definitions are described below:

- The system efficiency refers to the energy produced, based on the total energy input. This means that it does not only take the supplied heat into account, but also considers the energy supplied through pumps. To calculate this, the expression is shown in Equation 7.1:

$$\eta_{sys} = \frac{P_{turb}}{P_{pump} + Q_{in}} \tag{7.1}$$

  Using the system efficiency to rate the performance of the system makes it possible to examine how much of the supplied energy is actually converted to work. A low system efficiency would mean that the system is not very good at utilising the supplied heat and power.

- While the system efficiency might be low, the system might still produce more electricity than is supplied. To account for this, the COP is used as a measure of how much electricity is produced, relative to the amount supplied. The COP is calculated with Equation 7.2 and denotes the ratio between the power extracted from the turbine relative to the power supplied to operate the system.

$$COP = \frac{P_{turb}}{P_{pump}} \tag{7.2}$$

  This means that the difference between η_{sys} and COP lies in COP taking the supplied heat Q_{in} as "free" energy, which would mean the COP generally will be higher than the system efficiency.

7.2 Membrane Inlet Pressures

In Chapter 5 it was shown that both the feed and draw side pressures of the membrane plays an important role for membrane performance. It was found that the larger the pressure difference between the feed and draw side of the membrane, the higher the membrane power density. On the basis of these results, it would be logical that the same is true for the OHE, where the membrane is the governing component in relation to performance. However, due to the complexity and the fact that it is a closed system, unexpected behaviour may show. The outlet conditions of the membrane will ultimately affect the inlet conditions in the next iteration, which could alter the results relative to what was found from the membrane analysis. Table 7.1 shows the variation intervals for the inlet pressures on each side of the membrane.

Variable	Minimum value	Maximum value	Unit
Inlet feed pressure	10	45	[bar]
Inlet draw pressure	20	70	[bar]

Table 7.1: Variation interval of feed and draw inlet mass flow rates into the membrane.

The inlet feed pressure is dictated by the pressure loss in the hollow fibres. Although this can be set lower than 10 bar for some setups of the model, it is deemed a good balance such that the model remains stable and a realistic image is still provided of how the pressure in this regime affects the performance. Based on Table 7.1, Figure 7.1 shows how COP and system efficiency are affected by the pressures.

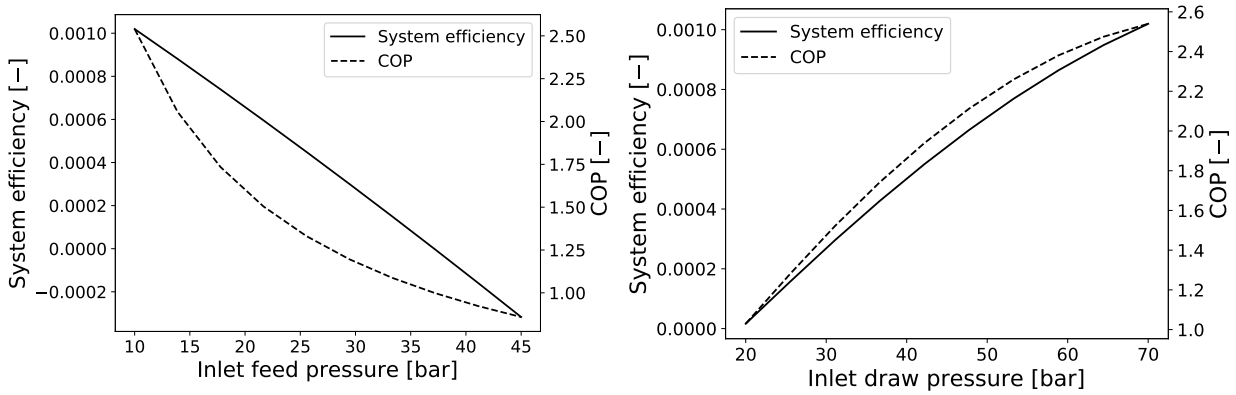

Figure 7.1: The left graph illustrates the efficiency and COP of the system as the pressure is varied on the inlet stream into the feed side of the membrane. The right graph illustrates the same parameters, but for variations on the inlet to the draw side of the membrane.

As shown in Figure 7.1, the pressures on both sides of the membrane matters significantly in regards to COP and system efficiency. Increasing the feed pressure results in a decrease of both the system efficiency and the COP of the system. This is the expected outcome, since the increase of feed pressure reduces the pressure difference, which is proportional to the water permeation. The same tendency shows when increasing the draw pressure, as this, opposedly to before, increases the pressure difference. From the left graph in Figure 7.1, it can also be seen that the COP drops significantly when the feed pressure is increased. This emphasises the importance of keeping the pressure on the feed side as low as possible. The same tendency shows for the draw pressure, however the change is not as significant.

7.3 Sink Temperatures

It is anticipated that the temperatures of the hot and cold sinks are crucial for the efficiency of the system. The larger the temperature difference, the more energy can be utilised. But it is not known how the sink temperatures affects the efficiency and the COP of the system. Therefore, understanding how the sink temperatures affect the efficiency of the OHE is of great interest, as this is crucial to determine where and if it makes sense to use this technology for waste heat recovery. To examine this, the temperatures of the hot and cold sinks are varied within the intervals described in Table 7.2.

Variable	Minimum value	Maximum value	Unit
Hot sink temperature	45	75	[°C]
Cold sink temperature	10	40	[°C]

Table 7.2: Variation interval of feed and draw inlet mass flow rates into the membrane.

As the scope of the project is to utilise low temperature waste heat, the hot sink temperature in Table 7.2 has been determined to be kept < 80°C. Based on the intervals in Table 7.2, the influence of the hot and cold sink temperatures is examined in Figure 7.2.

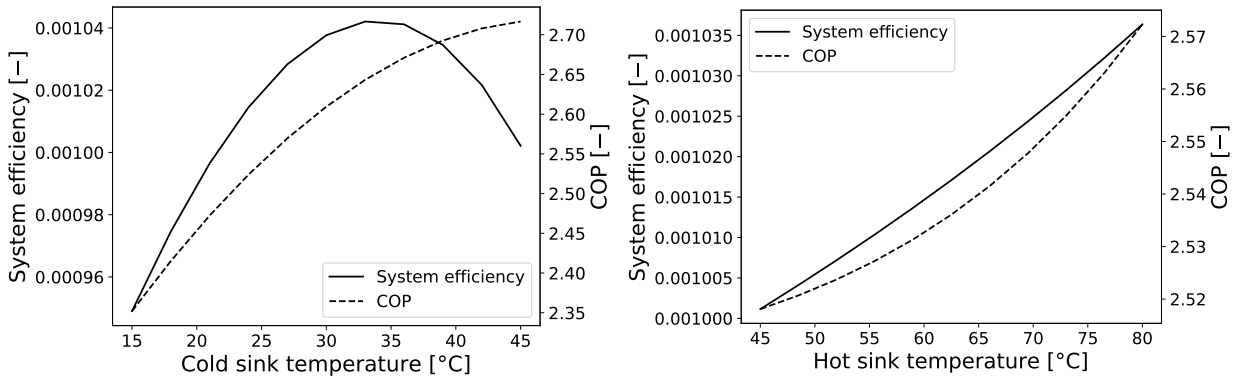

Figure 7.2: The left graph illustrates the efficiency and COP of the system as the temperatures of the hot and cold sinks are varied. The right graph illustrates the same parameters, but for variations on the inlet to the draw side of the membrane.

Figure 7.2 shows that increasing the temperature of the cold sink positively affects the system efficiency until it reaches around 35°C. Then, it starts decreasing again. The same tendency shows in regards to the COP. However, the peak COP seems to be reached at a higher temperature than what was the case for the efficiency. The positive proportionality that shows in terms of the cold sink temperature might be due to the fact, that increasing the temperature also increases the membrane permeation, as shown in Figure 4.7 in the validation of the model on page 25. With the way the model is constructed, the pressure in the evaporator is equal to the saturation pressure for the hot sink temperature. This means that increasing the hot sink temperature will reduce the pressure difference between the evaporator and the rest of the system. Neither the pumps nor the turbine are isentropic, so some of the energy supplied to these components will be transformed to heat. This practically means that the energy is lost from an efficiency and COP point of view. As the need for pumping work is reduced, less energy is wasted, leading to a higher system efficiency and COP.

7.4 Mass Flow Rates

In Chapter 5 it was shown that an increase of the mass flow on either side of the membrane will have a positive impact on the membrane performance. When modelling the full OHE system, pumps are used to circulate the fluid in the system. This also means that while the membrane model would benefit from as high mass flow rates as possible, this might not be the case for the model of the OHE. Increasing the mass flow rate will also result in increased pressure losses, which means the amount of power needed to pump the fluid is increased. To determine exactly to what extent the pressure loss affects the performance, the mass flow rates for both the feed and draw sides of the membrane are examined in the intervals noted in Table 7.3.

Variable	Minimum value	Maximum value	Unit
Inlet feed mass flow	0.5	2.5	[kg/s]
Inlet draw mass flow	0.5	2.5	[kg/s]

Table 7.3: Variation interval of feed and draw inlet mass flow rates into the membrane.

The results on COP and system efficiency by the variations denoted in the table can be seen in Figure 7.3.

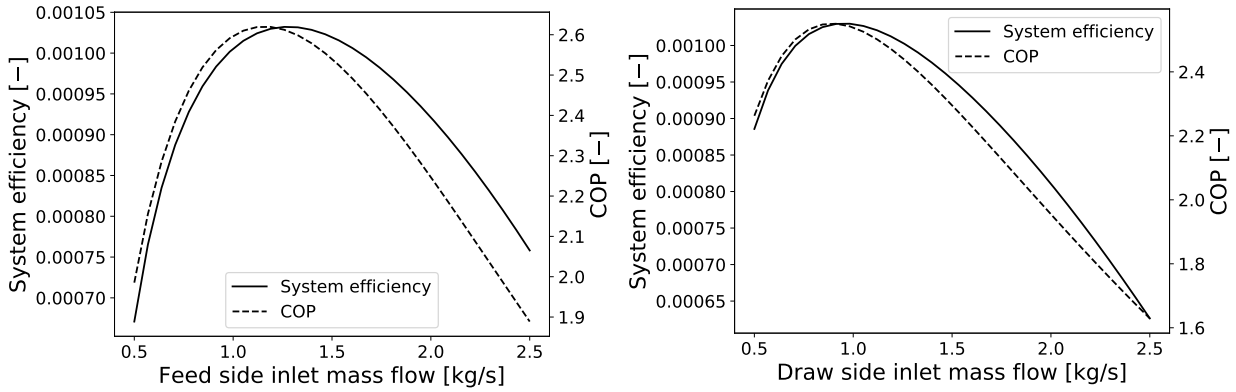

Figure 7.3: The left graph illustrates the efficiency and COP of the system as the inlet mass flow rates is varied into the feed side of the membrane. The right graph illustrates the same parameters, but for variations on the draw side of the membrane.

Figure 7.3 shows that when determining the appropriate feed and draw mass flows to maximise the performance of the OHE, the feed side flow rate should be higher than the flow rate on the draw side. The reasoning behind this is probably the much higher pressurisation on the draw side. This is because the high draw side pressurisation results in more power being required to pressurise the same amount of fluid on this side, relative to the feed side. It is also clear that the system does not benefit from neither very low nor very high flowrates, once again because high flowrate requires more pumping work, while lower flowrates result in a low mass transfer coefficient, which ultimately limits the permeation.

7.5 Concentrations

It was shown in the membrane analysis that the water permeation showed significant dependency to the concentration gradient over the membrane. As this is the case, it is of interest too exactly how much the system performance is affected by the concentrations. To examine the influence of the concentration on the draw side of the membrane, the inlet concentration is simply varied. However, for the feed side of the system, the concentration is dependent on the salt permeation over the membrane as well as the amount of fluid which is bypassed to the draw side. To how the feed concentration affects the system, the relationship between the bypass ratio and the feed concentration is therefore first to be understood. This is examined in Figure 7.4.

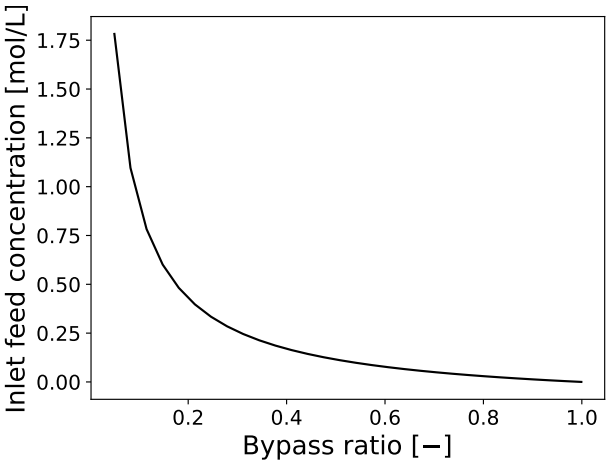

Figure 7.4: Relationship between the bypass ratio and the feed concentration.

As shown in Figure 7.4, the feed concentration decreases as the bypass ratio is increased. This is the expected behaviour, as an increase to the bypass flow reduces the amount of salt which is recirculated on the feed side. When the bypass ratio reaches 1, where the full flow is directed to the draw side, no salt will accumulate on the feed side, as there no longer exists recirculation. As the bypass ratio dictates the concentration on the feed side, this is varied instead of the feed concentration. The variation intervals of this and the membrane inlet concentration on the draw side are listed in Table 7.4.

Variable	Minimum value	Maximum value	Unit
Bypass ratio	0.05	0.999	[−]
Inlet draw concentration	2.5	6	[mol/L]

Table 7.4: Variation interval of feed and draw inlet mass flow rates into the membrane.

As can be seen in Table 7.4, the bypass ratio is only varied up to 0.999. This is because of the way the model is constructed, as it would make the model diverge to increase the bypass to 1. However, Figure 7.4 shows that the difference between a bypass ratio of 0.999 and 1 is very small, so it is deemed negligible. The results of the variations can be seen in Figure 7.5 on page 47.

As can be seen on figure 7.5, both system efficiency and COP are very dependent on the bypass ratio. This suggests that the salt concentration on the feed side of the membrane is of

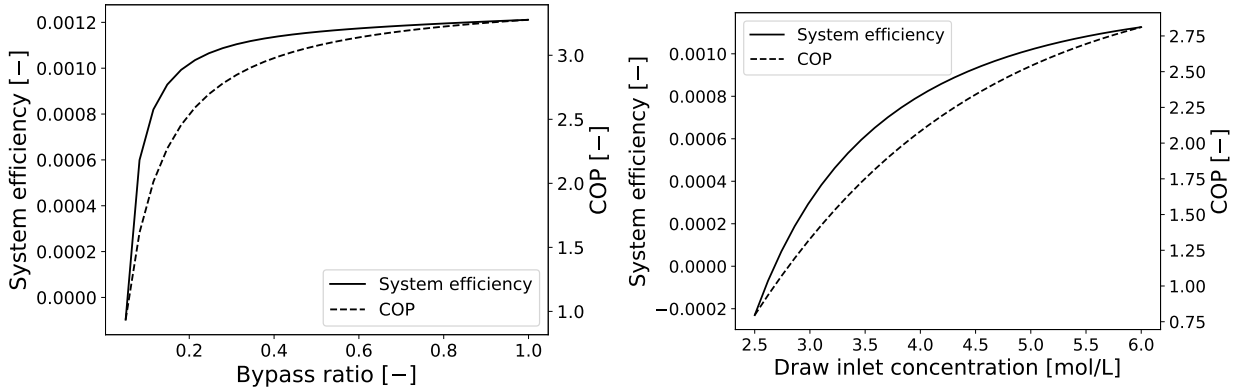

Figure 7.5: The left graph illustrates the efficiency and COP of the system as the bypass ratio is varied. The right graph illustrates the same parameters, but for variations on the draw concentration at the inlet to the membrane.

such significance, that the best solution is just to resupply with pure water and recirculate no fluid. This is the case, even though it results in some potential for power generation being lost through the bypass stream.

As expected, the inlet draw concentration shows the opposite trend. This behaviour also makes sense as an increase of the draw concentration increases the concentration difference from the feed to the draw side, hence increasing the osmotic pressure difference.

Based on the analysis of the OHE system, a short summary follows in the next section, along with an optimisation based on the results of the analysis.

7.6 Key Takeaways and Optimisation

Through the system analysis, it was found that the system generally behaves as expected with regards to concentrations and pressures. The closer the pressure difference is to the maximum power density as shown in Figure 4.2 on page 18, the better the system performs. Furthermore, large concentration differences show the same results.

Increasing the mass flow rates also have a positive effect on the performance, at least up to a certain point. As predicted after the membrane analysis of the mass flow rates in Figure 5.5 on page 31, it is because the increase of pressure loss eventually grows larger than the increase of mass transfer coefficients, which means the pumping power becomes too significant for the system to be feasible. Similar trends emerged as for the membrane analysis, but without considering the increased supply of power to accommodate the pressure loss, the membrane performance was well served by the increased mass flow rates, which is not the case in the system analysis.

The most surprising effect showed with the variation in the temperature of the hot sink. While the direction of change was as expected, the rate of change of the hot sink temperature was lower than anticipated. While the hot sink temperature also affects the performance of the system, the effect is much less significant when compared to the rest of the modelled parameters.

Based on the analysis of the system parameters, an optimisation is conducted with the purpose of examining exactly how good the system can perform with the design proposed in Figure 6.4. The ideal solution would be to optimise all the parameters that have been examined. However, because of computational limitations, that will be too comprehensive. Therefore it must be determined which parameters have the largest potential for improvement.

Figure 7.1 on page 43 shows that the feed pressure should be as low as possible for the given setup, and the draw pressure should be as high as possible. Previously mentioned in Section 5.6, the draw side pressure is limited to 70 bar, due to limitations in the membrane, and the feed pressure should not go below 10 bar, as this will jeopardise the stability of the model. The pressures will therefore not be optimised, since this is the same value as are already used. To examine the behaviour of internal parameters, the temperatures are kept constant. This leaves the following variables for optimisation:

1. Draw concentration
2. Bypass ratio
3. Feed side mass flow rate
4. Draw side mass flow rate

To ensure the viability of the listed parameters in terms of what to optimise, a tornado chart is constructed. The tornado chart shows the relative change of COP, as function of 1% increase or decrease in the given parameter. For example, if the bypass ratio starts at 0.2, it is varied to 0.198 and 0.202. If the COP changes from 3 to 3.06, with the increase of bypass flow, that will be equal to a relative change of 1.02. The results of this examination are shown in Figure 7.6.

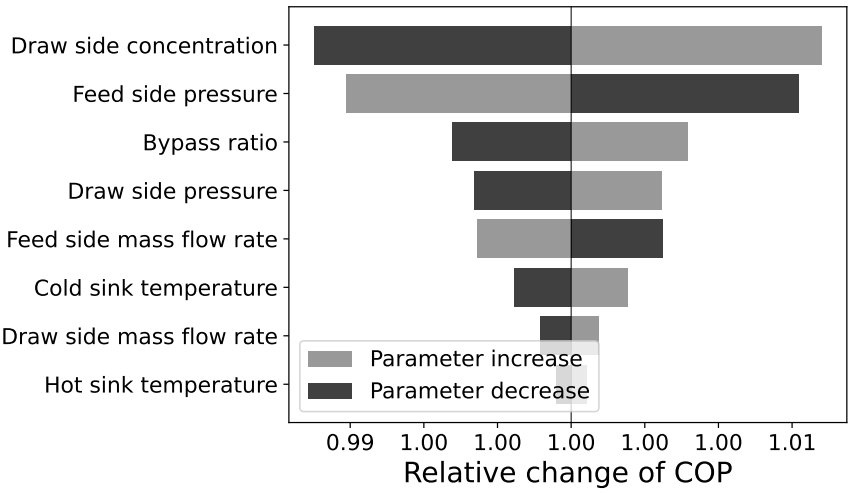

Figure 7.6: Comparison of the impact on COP from each varied parameter. The parameters are increased and decreased with 1% of their value to examine the relative change of COP.

As can be seen from Figure 7.6, the most important effects are the concentration on the draw side of the membrane and the feed side inlet pressure, which seem to be of greater significance than the rest of the parameters. It is however to be noted that both the bypass ratio and the feed side mass flow rate also seem to be significant, which makes these parameters good candidates for optimisation. It is expected that when the feed side mass flow rate is changed, the optimal point for the draw side mass flow rate will also change. Therefore, it makes sense to optimise both these parameters. The optimisation is performed in Python, and uses the algorithm *Limited Memory Broyden-Fletcher-Goldfarb-Shanno* (L-BFGS), as Python documentation recommends this algorithm for unconstrained nonlinear optimisation problems. (SciPy 2024)

If given, the algorithm uses a user-defined gradient to achieve faster convergence. However, in cases such as this where the gradient is not given, it uses finite differences to determine the

gradient. While the normal L-BFGS algorithm cannot handle bounds, a variant of the algorithm is proposed in Byrdt et al. (1995). This variant is called L-BFGS-B, with '-B' meaning it is designed to handle bounds. This is the variant of the algorithm chosen for the optimisation. The setup for the optimisation and the results can be seen in Table 7.5.

Setup			
Variable	Minimum value	Maximum value	Unit
Bypass ratio	0.05	1.00	[−]
Inlet draw concentration	1.00	6.00	[mol/L]
Feed side mass flow rate	0.50	3.00	[kg/s]
Draw side mass flow rate	0.50	2.50	[kg/s]
Results			
Variable	Optimised value		Unit
Bypass ratio	1.00		[−]
Inlet draw concentration	6.00		[mol/L]
Feed side mass flow rate	1.37		[kg/s]
Draw side mass flow rate	0.62		[kg/s]
Power produced	5.90		[kW]
COP	3.46		[−]
Thermal efficiency	0.0013		[−]

Table 7.5: Variation interval of feed and draw inlet mass flow rates into the membrane.

In Table 7.5, both the bypass ratio and the inlet draw concentration behaved as expected, as the difference of the solute concentrations over the membrane reached the allowed maximum. In terms of mass flow rates, the trend is similar to when varied in Chapter 7. Once again, it seems that the feed side mass flow should be larger than the draw side mass flow under optimal conditions. Furthermore, it is clear that optimising the system did improve the efficiency, but it is still well below 1%. The COP also improved, reaching 3.46.

As the optimal conditions for the model has now been found, it is of relevance to determine how the decisions related to the model setup has affected the results. More detail on this is given in the chapter following.

Chapter 8

Discussion

In Section 4.2, a list of assumptions was stated, which reduced the complexity of the model. However, by doing so, it also leads to the consequence that the accuracy of the model has been reduced. In the model, some assumptions are aimed towards the components, while others focus on the properties of fluids.

Component assumptions

The PEX was modelled such that the efficiency of the component affected only the leakage flow, as this made the modelling of the PEX much simpler. In reality, efficiency is also affected by friction and some mixing inside each pipe as they rotate between the high- and low-pressure sides. This means that for an actual PEX, the efficiency loss is not only governed by leakage flow, but also by the additional work to account for the other losses. As mentioned in Section 6.2, the leakage flow only accounts for 1-2% of the loss. As different property models were used for the pure water and the saline solution, the enthalpy reference states for the fluids were not consistent. As this was the case, it was difficult to construct the membrane model such that it could handle a temperature difference between the feed and draw sides. This led to the decision that the temperatures on the coolers should be the same. Although this does not directly affect the model, it creates a limitation in regards to the system parameters that can be examined.

As stated in Section 1.1, the temperature on the draw side has a greater effect on the membrane performance than the temperature on the feed side. If the temperatures could be changed individually, the system performance might have seen more improvement.

The model was constructed with the total efficiency of the pumps set at 0.8 and the efficiency of the turbine set to 0.9. While documentation on the turbine efficiency has been provided, this is not the case for pump efficiency. Therefore, the large differential pressure over the pumps might mean, that the efficiency of 0.8 is too optimistic. To examine the effects of the assumption, Figure 8.1 shows how the system efficiency and the COP are affected by variations to pump efficiency.

Figure 8.1 on page 51 shows that the pump efficiency is very important for the overall system performance. This is also as expected, since the generated electricity is "only" around 3 times as high as the energy input into the pumps. Changing the efficiency from 0.8 to 0.5 means that about 1.5 times as much power must be supplied to run the system, hence showing significant effects to system efficiency and COP.

In Chapter 4 it is mentioned that the membrane model is built up with membrane properties from an article, and the dimensions of the membrane and shell coming from a datasheet from

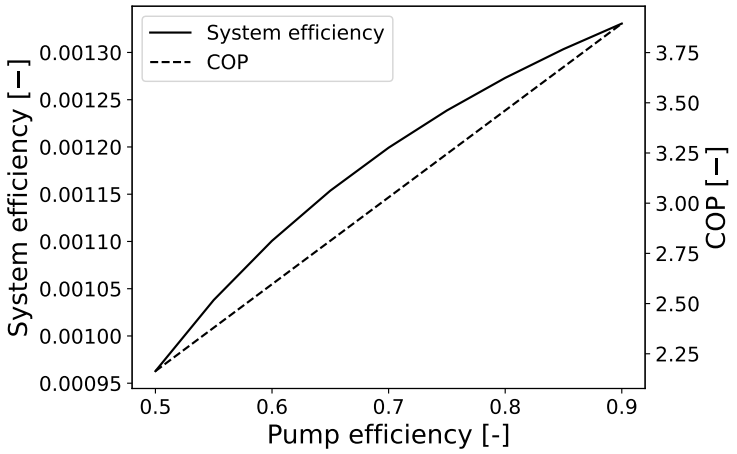

Figure 8.1: System efficiency and COP as functions of the pump efficiencies.

the manufacturer. This might result in some uncertainties as it is unsure whether the data is actually from the exact same type of membrane. Changing the properties or the dimensions of the membrane will also yield different results of the report, however it is still expected that the parameters used in the project are within range of what is realistic.

Fluid Assumptions

In the model, several assumptions are also made in terms of the saline solution. It is assumed that no precipitation of salt will occur in the system. Since pure water is separated from the solution by destillation, some salt might precipitate in this process forming salt deposits on the heating coil in the evaporator, which inevitably will reduce the efficiency, leading to higher required thermal loads to achieve the same results. In addition, salt precipitation is also expected inside the membrane. Over longer periods of time, this will clog the pores in the membrane. This leads to increased flow resistance through the membrane, meaning that the permeation will ultimately decrease. To accommodate this, the membrane will need to be replaced at some point, based on how much fouling occurs. As the model examines the system in steady state, this was neglected as it has no impact on the instantaneous modelling results.

Feasibility

The optimised efficiency of the OHE turned out to be around 0.00074 with a COP of 4.1. This means, that while the system is not very effective at using the supplied waste heat, it does however still produce more electricity than is added to the system. As the waste heat would not be utilised without some type of heat recovery system, it can be argued that as long as more electricity is produced than what is used, the system makes sense, at least from an energy output scope. However, it should be noted that for the modelled system to produce 6 kW of energy, about 1.34 kg/s is evaporated. For a hot sink temperature of 65°C, the density at saturation pressure is $\approx$ 0.16 kg/m^3. This means that a flow of 9 m^3/s leaves the evaporator to pass through. For this to be possible, the coolers and the evaporator must be of a certain size. The size of these components would also scale with the power output of the system.

Chapter 9

Conclusion

This project has examined the use of PRO for ultra low temperature waste heat recovery. This project examines this through the use of an OHE with NaCl as the solute. While several technologies are already being examined and tested for the purpose, the knowledge about OHEs is limited, especially when using NaCl as the solute.

To examine the performance of the system, an analysis was made of the membrane and how that was affected by variations of parameters with power density and reverse salt flux as performance parameters to evaluate how the desired properties for PRO are affected by the parameter variations. From the membrane analysis, it was determined that for PRO to be used in an OHE, a bypass stream is necessary. The purpose of this stream is to circulate the salt, which has permeated through the membrane to the feed side, back to the draw side of the membrane such that salt does not accumulate on the feed side of the membrane.

On the basis of the results of the membrane model, the entire OHE system was examined. The focus of the system analysis was to examine the behaviour of the system efficiency and the COP of the system. Lastly, an optimisation was performed to evaluate how well the system can perform with the layout proposed in the project.

In the optimisation, the highest system efficiency reached was ≈ 0.0013, or equal to 0.13%. This means that about 750 times more heat is needed than the amount of electricity produced. Due to this, the heat has to be practically free, as even relatively low heating prices will mean that the system will likely not be feasible.

Meanwhile, the COP of the optimised system is ≈ 3.46, so more electricity is still produced than consumed by the system. It is though important to note that the flow through the pure water cooler is around 9 m^3/s. This means that a very large cooler would be necessary to accommodate the flow. The same is true for the evaporator, as great volumes of steam are produced in this component.

As mentioned in Chapter 1, several other technologies are also being researched for waste heat recovery in the same temperature intervals as where the NaCl based OHE is proposed. This means that for this system to be a good candidate, significant resources should be invested in improving the system. Improvements are necessary in terms of both system efficiency and finding a way to reduce the size of the components, since this especially proposes a major issue, both in regards to required space and the fact that components of this size will be expensive when considering the pressures that have to be endured.

Chapter 10

Suggestions for Future Work

Based on the findings of the project and the stated conclusion, the following areas for future work have been identified.

10.1 Improvements to the System Design

As stated in Chapters 8 and 9, the system efficiency is relatively low. A significant part of the reason for this is the fact, that the water is evaporated to create the pure water stream, which is energy intensive. Just after the evaporation, the steam cooled and recondensed as the membrane cannot withstand such temperatures. Because the pressure in the cooler and the evaporator is similar, there is no temperature difference between them. That means that the heat from the cooler cannot be used for the evaporator, as can be seen in the pinch analysis in Figure 10.1

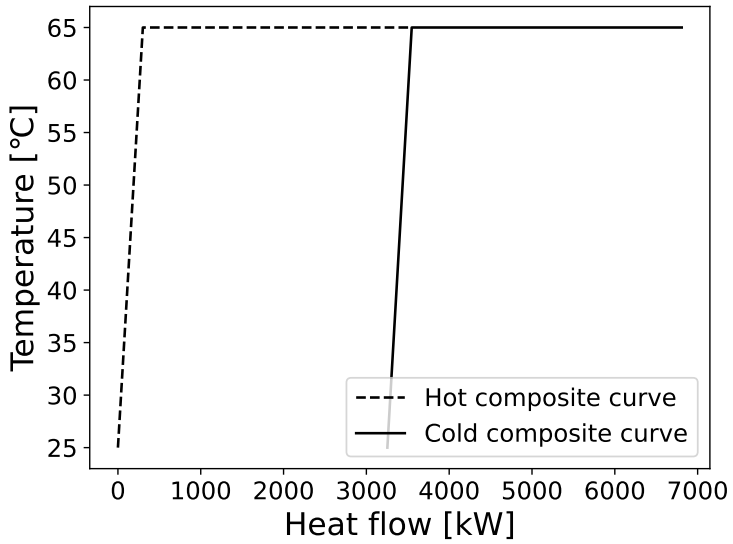

Figure 10.1: Pinch analysis of the optimised OHE system. The graph shows the cold and the hot composite curves.

As can be seen in Figure 10.1, the overlap where the energy from the cooler can be used to heat the flow in the evaporator is small, compared to the total energy used. By increasing the overlap, the system efficiency would also increase significantly. A proposal to doing this would be to investigate if a compressor before the pure water cooler would be too energy consuming, as this would increase the pressure in the cooler, thereby increasing the saturation temperature.

This would allow using the energy from the condensation directly to evaporate the water. In Figure 10.1, the horisontal line of the hot composite curve shows the energy required to evaporate the water. If the energy from condensation were used to evaporate the fluid in the evaporator, this line would disappear, resulting in a great decrease to the necessary heating.

10.2 Different Solutes

As stated in the previous section, the water has to be evaporated to produce the stream of pure water. Since water has a relatively high enthalpy of vaporisation, large amounts of heat must be supplied to achieve this. Furthermore, the boiling point of water at atmospheric pressure is 100°C, which means the pressure has to be sub-atmospheric to reach an appropriate boiling point. By using another solute, which has a lower boiling point than water, the pressure does not have to be decreased to the same extent. Furthermore, the chosen solute might have a lower enthalpy of vaporisation, meaning that less heat must be applied to the solution.

10.3 Electricity Grid Regulation and Dynamic System Model

With the green transition in progress, the share of renewable electricity increases. Since the renewable sources generally are more unstable in terms of production than fossil energy production, more effort must be used in stabilising the grid. This is done through so called ancillary services, where electricity suppliers are compensated for regulating the production of their facilities to aid with the stabilisation. In Denmark, the ancillary services are separated based on the reaction time and the amount of regulation supplied. This also heavily affects the compensation to the supplier. (Energinet 2024)

With the amounts of ultra low temperature waste heat available, it would be interesting to examine how this could affect the feasibility of the system, as the expected outcome would be that it would improve the business case.

In the case that grid regulation becomes relevant to the business case of the system, a dynamic model of the system would also be relevant. As the necessary ancillary services vary, the instantaneous feasibility of running the system will also change. In this relation, it is also of interest to understand how the system is affected dynamically by changes to external parameters, as it might have positive or negative effects on the system performance.

10.4 Upgrading the model

The membrane model used in this project is partly based on observations of experiments, where theoretical models have been fitted to the results. If the circumstances for the membrane deviates from those under which the experiments were conducted, some error might occur. To overcome this, a model using computational fluid dynamics (CFD) could be constructed, which would be expected to reduce the error even further. The same goes for other components in the system. As previously stated, the PEX is simplified such that the efficiency only accounts for leakage flow. This is an assumption which is expected to be fairly insignificant, but by doing so, other effects might be induced which affect the results.

By taking these steps, the number of assumptions will be reduced. However, reducing the number of assumptions in the model will only increase the accuracy of the results. For the system to be feasible, the other suggestions for future work will be of greater priority.

References

Bevacqua, M. et al. (Oct. 2016). "Performance of a RED system with ammonium hydrogen carbonate solutions". In: *Desalination and Water Treatment* 57.48-49, pp. 23007–23018. ISSN: 19443986. DOI: 10.1080/19443994.2015.1126410.

Bhinder, Amrit, Simin Shabani, and Mohtada Sadrzadeh (Mar. 2018). "Effect of Internal and External Concentration Polarizations on the Performance of Forward Osmosis Process". In: *Osmotically Driven Membrane Processes - Approach, Development and Current Status*. InTech. DOI: 10.5772/intechopen.71343.

Byrdt, Richard H et al. (1995). *A LIMITED MEMORY ALGORITHM FOR BOUND CONSTRAINED OPTIMIZATION**. Tech. rep. 5, pp. 1190–1208. URL: https://epubs.siam.org/terms-privacy.

Cengel, Yunus A., John Cimbala, and Robert H. Turner (2017). *Fundamentals of Thermal Fluid Sciences*. 5th ed. McGraw-Hill Education. ISBN: 978-9-814-72095-3.

Chintalacheruvu, Sanjana, Yiyang Ren, and Jonathan Maisonneuve (June 2023). "Effectively using heat to thermally enhance pressure retarded osmosis". In: *Desalination* 556. ISSN: 00119164. DOI: 10.1016/j.desal.2023.116570.

Dixon, S. L. and C. A. Hall (2014). *Fluid Mechanics and Thermodynamics of Turbomachinery*. 7th ed. Elsevier Inc., pp. 364–366. ISBN: 978-0-12-415954-9.

DXP Pacific (2023). *Peristaltic vs Centrifugal Pumps: Differences to understand*. URL: https://dxppacific.com/peristaltic-vs-centrifugal-pumps-differences-to-understand/.

Einarsson, Sigurður John and Bing Wu (Feb. 2021). *Thermal associated pressure-retarded osmosis processes for energy production: A review*. DOI: 10.1016/j.scitotenv.2020.143731.

Energinet (2024). *INTRODUKTION TIL SYSTEMYDELSER*. Tech. rep.

Energy Recovery (2020). *Youtube: Inside Energy Recovery's PX® Pressure Exchanger®*. URL: https://www.youtube.com/watch?v=IBwkgrwZYNU&ab_channel=EnergyRecovery.

— (2024). *HIGH-PRESSURE PX*. URL: https://energyrecovery.com/pressure-exchangers/high-pressure-px/.

Galamba, N. (May 2012). "Mapping structural perturbations of water in ionic solutions". In: *Journal of Physical Chemistry B* 116.17, pp. 5242–5250. ISSN: 15205207. DOI: 10.1021/jp3014578.

Geankoplis, Christie John (2003). *Transport Processes and Separation Process Principles*. 4th ed. Pearson Education Limited. ISBN: 9781292026022.

Gonzales, Ralph Rolly et al. (Mar. 2021). "Salinity gradient energy generation by pressure retarded osmosis: A review". In: *Desalination* 500. ISSN: 00119164. DOI: 10.1016/j.desal.2020.114841.

IEA (2023a). *Data Centres and Data Transmission Networks*. URL: https://www.iea.org/energy-system/buildings/data-centres-and-data-transmission-networks#tracking.

— (2023b). *Denmark 2023 - Energy Policy Review*. Tech. rep. URL: www.iea.org.

Kim, Jungwon et al. (Nov. 2015). "Evaluation of apparent membrane performance parameters in pressure retarded osmosis processes under varying draw pressures and with draw solutions containing organics". In: *Journal of Membrane Science* 493, pp. 636–644. ISSN: 18733123. DOI: 10.1016/j.memsci.2015.07.035.

Kumar, Prashant et al. (Oct. 2019). "Shape memory alloy engine for high efficiency low-temperature gradient thermal to electrical conversion". In: *Applied Energy* 251. ISSN: 03062619. DOI: 10.1016/j.apenergy.2019.05.080.

Liang, Yingzong et al. (Nov. 2022). "A systematic methodology for targeting the thermodynamic limit of pressure-retarded osmosis with non-zero driving force". In: *Journal of Cleaner Production* 375. ISSN: 09596526. DOI: 10.1016/j.jclepro.2022.133905.

Luberti, Mauro et al. (Jan. 2022). "An estimate of the ultralow waste heat available in the European Union". In: *Energy* 238. ISSN: 03605442. DOI: 10.1016/j.energy.2021.121967.

Luo, Xi et al. (June 2012). "Power generation by coupling reverse electrodialysis and ammonium bicarbonate: Implication for recovery of waste heat". In: *Electrochemistry Communications* 19.1, pp. 25–28. ISSN: 13882481. DOI: 10.1016/j.elecom.2012.03.004.

Madsen, Henrik T. et al. (2017). "Pressure retarded osmosis from hypersaline solutions: Investigating commercial FO membranes at high pressures". In: *Desalination* 420, pp. 183–190. ISSN: 00119164. DOI: 10.1016/j.desal.2017.06.028.

McCutcheon, Jeffrey R., Robert L. McGinnis, and Menachem Elimelech (July 2006). "Desalination by ammonia-carbon dioxide forward osmosis: Influence of draw and feed solution concentrations on process performance". In: *Journal of Membrane Science* 278.1-2, pp. 114–123. ISSN: 03767388. DOI: 10.1016/j.memsci.2005.10.048.

McGinnis, Robert L., Jeffrey R. McCutcheon, and Menachem Elimelech (Nov. 2007). "A novel ammonia-carbon dioxide osmotic heat engine for power generation". In: *Journal of Membrane Science* 305.1-2, pp. 13–19. ISSN: 03767388. DOI: 10.1016/j.memsci.2007.08.027.

Micheli, Diego, Mauro Reini, and Rodolfo Taccani (Feb. 2021). "Thermodynamic analysis of a Carbon Carrier Cycle (CCC) for low temperature heat recovery". In: *E3S Web of Conferences*. Vol. 238. EDP Sciences. DOI: 10.1051/e3sconf/202123801002.

Munubarthi, Kranthi Kumar et al. (Dec. 2020). "Distributed parameter system modeling approach for the characterization of a high flux hollow fiber forward osmosis (HFFO) membrane". In: *Desalination* 496. ISSN: 00119164. DOI: 10.1016/j.desal.2020.114706.

Oltmanns, Johannes et al. (May 2020). "Potential for waste heat utilization of hot-water-cooled data centers: A case study". In: *Energy Science and Engineering* 8.5, pp. 1793–1810. ISSN: 20500505. DOI: 10.1002/ese3.633.

Palenzuela, Patricia et al. (Dec. 2018). "Performance analysis of a red-med salinity gradient heat engine". In: *Energies* 11.12. ISSN: 19961073. DOI: 10.3390/en11123385.

Pavuluri, Saideep (2014). *Kinetic approach for modeling salt precipitation in porous-media*. Tech. rep. URL: https://www.researchgate.net/publication/262495450.

Rahman, Sumaita Nawar, Haleema Saleem, and Syed Javaid Zaidi (Mar. 2023). *Progress in membranes for pressure retarded osmosis application*. DOI: 10.1016/j.desal.2022.116347.

SaltPower (2024). *SaltPower - Turning salt into green and clean energy*. URL: https://www.saltpower.net/markets-we-serve/.

Sawamura, Seiji et al. (June 2007). "Solubility of sodium chloride in water under high pressure". In: *Fluid Phase Equilibria* 254.1-2, pp. 158–162. ISSN: 03783812. DOI: 10.1016/j.fluid.2007.03.003.

SciPy (2024). *Optimization (scipy.optimize)*. URL: https://docs.scipy.org/doc/scipy/tutorial/optimize.html#unconstrained-minimization-of-multivariate-scalar-functions-minimize.

Shibuya, Masafumi et al. (Apr. 2015). "Effect of operating conditions on osmotic-driven membrane performances of cellulose triacetate forward osmosis hollow fiber membrane". In: *Desalination* 362, pp. 34–42. ISSN: 00119164. DOI: 10.1016/j.desal.2015.01.031.

Stover, Richard L (2005). *ENERGY RECOVERY DEVICE PERFORMANCE ANALYSIS*. Tech. rep. URL: www.energy-recovery.com.

Toyobo (2023a). *FO: Toyobo MC Membrane Module for Forward Osmosis*.

— (2023b). "Toyobo MC: Membrane Module for Brine Concentration". In.

U.S. Energy Information Administration (2023). *INTERNATIONAL: Electricity*. URL: https://www.eia.gov/international/data/world/electricity/electricity-consumption?pd=2&p=0000002&u=0&f=A&v=mapbubble&a=-&i=none&vo=value&t=C&g=none&l=249--12&s=315532800000&e=1640995200000&.

United Nations (2023). *The Paris Agreement*. URL: https://unfccc.int/process-and-meetings/the-paris-agreement.

Yoshikawa, Shiro, Kohei Ogawa, and Shinichi Minegishi (1994). "Distributions of pressure and flow rate in a hollow-fiber membrane module for plasma separation." In: *JOURNAL OF CHEMICAL ENGINEERING OF JAPAN* 27.3, pp. 385–390. ISSN: 0021-9592. DOI: 10.1252/jcej.27.385.

Al-Zainati, Nahawand et al. (Mar. 2024). "Multiple staging of pressure retarded osmosis: Impact on the energy generation". In: *Desalination* 573. ISSN: 00119164. DOI: 10.1016/j.desal.2023.117199.